Advancements in the Split Hopkinson Bar Test

by

Michael Adam Kaiser

Thesis submitted to the Faculty of the Virginia Polytechnic Institute and State University in partial fulfillment of the requirements for the degree of

Master of Science

in

Mechanical Engineering

Dr. Alfred Wicks, Chairman

Leonard Wilson

Dr. William Saunders

May 1, 1998

Blacksburg, Virginia

Keywords: Hopkinson Bar, High Strain-Rate, Impact Testing, Wave Dispersion, Bar Impedance, NSWCDD

Advancements in the Split Hopkinson Bar Test

by

Michael Adam Kaiser

(ABSTRACT)

The split Hopkinson bar test is the most commonly used method for determining material properties at high rates of strain. The theory governing the specifics of Hopkinson bar testing has been around for decades. It has only been the last decade or so, however, that significant data processing advancements have been made. It is the intent of this thesis to offer the insight of its author towards new advancements.

The split Hopkinson bar apparatus consists of two long slender bars that sandwich a short cylindrical specimen between them. By striking the end of a bar, a compressive stress wave is generated that immediately begins to traverse towards the specimen. Upon arrival at the specimen, the wave partially reflects back towards the impact end. The remainder of the wave transmits through the specimen and into the second bar, causing irreversible plastic deformation in the specimen. It is shown that the reflected and transmitted waves are proportional to the specimen's strain rate and stress, respectively. Specimen strain can be determined by integrating the strain rate. By monitoring the strains in the two bars, specimen stress-strain properties can be calculated.

Several factors influence the accuracy of the results, including longitudinal wave dispersion, impedance mismatch of the bars with the specimens, and transducer properties, among others. A particular area of advancement is a new technique to determine the bars dispersive nature, and hence reducing the distorting effects. By

implementing numerical procedures, precise alignment of the strain pulses is facilitated. It is shown that by choosing specimen dimensions based on their impedance, the transmitted stress signal-to-noise ratio can be improved by as much as 25dB. An in depth discussion of realistic expectations of strain gages is presented, along with closed form solutions validating any claims. The effect of windowing on the actual strains is developed by analyzing the convolution of a rectangular window with the impact pulse.

The thesis concludes with a statistical evaluation of test results. Several recommendations are then made for pursuing new areas of continual research.

ACKNOWLEDGEMENTS

First and foremost I would like to express my deepest thanks to my parents and sister. To my dad for teaching me to question things and to my mom for never doubting my answers. Seeing my sister's hard work be so handsomely rewarded has been an inspiration. Their continual support and encouragement has been unending and unconditional, as is my love for them. The only repayment I can offer is to extend the same love and devotion to my own children.

This thesis represents a culmination of hundreds of hours of work by its author, Leonard Wilson of the Naval Surface Warfare Center, Dr. Alfred Wicks from Virginia Tech, and many previous investigators. I would like to thank Leonard and Dr. Wicks for their insight and encouragement. Dr. Wicks helped redirect my Masters thesis from what could have been an unpleasant experience. Leonard has been a joy to work for, always able to see eye to eye with me on the project. I would like to thank Dr. William Saunders for taking the time to review my thesis. I would also like to thank Monica for all of her love and understanding, never sacrificed by her own treacherous schedule. Though they probably don't know it, these people have helped me define myself as a person in just the past two years. Thanks to all of you, I appreciate everything you have done for me.

CONTENTS

LIST OF ILLUSTRATIONS

LIST OF TABLES

CHAPTER 1

OVERVIEW OF SPLIT HOPKINSON

BAR TEST

1.1 INTRODUCTION

The design of structures is based almost solely on tabulated material data, usually in the form of a stress-strain diagram. Optimal designs require accurate and complete tables for materials tested under a variety of conditions. The majority of available tabulated material properties were gathered by deforming the specimen very slowly. According to Shigley & Mitchell [1], "the average strain rate used in obtaining the stress-strain diagram is about 0.001 in-s/in or less." It has been known for years that materials are stronger at higher rates of strain, such as caused by an impact. The behavior of structures to impacts has been of interest to many engineers for purposes of design as well as developing constitutive models of the materials tested.

The split Hopkinson bar apparatus has quickly become the most widely used device to test materials at high strain rates. Though integral to the research presented in this thesis, the purpose of this thesis is not to test materials at high strain rates. Rather it is to introduce improvements to the current testing techniques and data processing currently employed in split Hopkinson bar testing.

Over the past two years, the Naval Surface Warfare Center Dahlgren Division along with Virginia Tech has been building up a program for split Hopkinson bar testing. The facility is now equipped to perform compression tests on a wide range of materials while employing the latest in data acquisition and data processing techniques. The author would not be at all surprised to see NSWCDD's Hopkinson bar program become a leader in high strain rate testing.

1.2 FUNDAMENTALS OF HOPKINSON BAR TESTING

The split Hopkinson bar test is the most commonly used method for determining material properties at high rates of strain. Significant advancements implemented from the areas of testing techniques, numerical methods, and signal processing have

improved the accuracy and repeatability of high strain rate testing. Constant strain rate tests can be performed at strain rates approaching $10^4\ s^{-1}$ relatively easily.

In the split Hopkinson bar test, a short cylindrical specimen is sandwiched between two long elastic bars, as shown in figure 1.1. The bars are generally made of a high strength maraging steel with diameters less than 0.75" and a length near five feet.

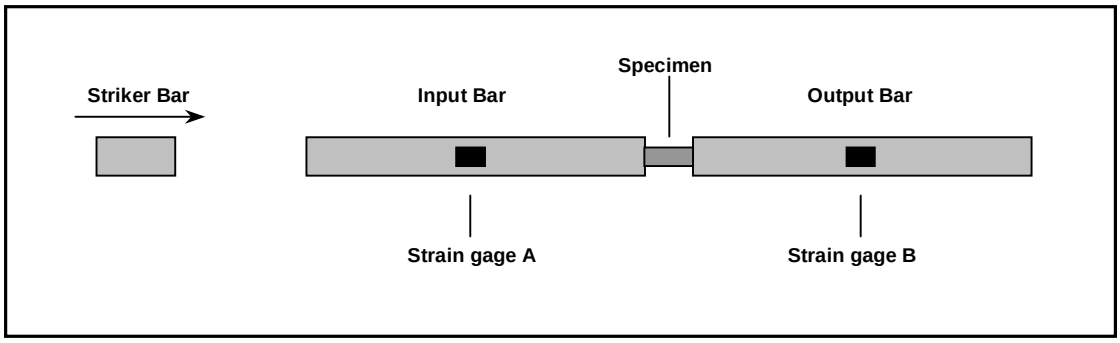

Figure 1.1 Schematic of Split Hopkinson bar Apparatus

Ballpark specimen dimensions are ¼" diameter and ¼" length. The ends of the pressure bars and specimen are machined flat to enforce prescribed boundary conditions. Typically a projectile (striker bar) is fired into the end of the input bar generating a compressive stress pulse. Immediately following impact, this pulse travels along the bar towards the input bar-specimen interface at which the pulse is partially reflected into the input bar and partially transmitted through the specimen and into the output bar. The reflected pulse is reflected as a wave in tension, whereas the transmitted pulse remains in compression. The strain histories in the two pressure bars are recorded by strain gages A and B.

So long as the pressures in the bars remain under their elastic limits, specimen stress, strain, and strain rate may be calculated from the recorded strain histories. Under certain deformation conditions, qualified later, only two important strain pulses need be identified. These are the reflected pulse and the pulse transmitted through the

specimen. Kolsky [2] developed the following relation for calculating the specimen stress.

$$\sigma_s(t) = E\frac{A_o}{A}\varepsilon_T(t) \tag{1.1}$$

where E is the output pressure bar's elastic modulus, A_o is the output bars cross sectional area, A is the sample's cross sectional area, and $\varepsilon_T(t)$ is the transmitted strain history. Specimen strain rate may be calculated from

$$\frac{d\varepsilon_s(t)}{dt} = -\frac{2C_o}{L}\varepsilon_R(t) \tag{1.2}$$

where $\varepsilon_R(t)$ is the reflected input bar strain history, L is the specimen length prior to impact, and C_o is the infinite wavelength wave velocity in the input pressure bar, calculated from elementary vibrations as

$$C_o = \sqrt{\frac{E}{\rho}} \tag{1.3}$$

where E and ρ are the bars elastic modulus and density, respectively. Equation 1.2 can be integrated in time to yield the specimens strain, given by Equation 1.4.

$$\varepsilon_s(t) = -\frac{2C_o}{L}\int_0^t \varepsilon_R(t)dt \tag{1.4}$$

Though these equations have been around since the late 40's, it has only been in the last decade or so that significant data processing advancements have been possible, mainly due to high-speed computers. FFT analysis and other numerical procedures can be completed quickly on a PC based machine.

1.3 COMPLICATIONS WITH TESTING AND DATA PROCESSING

As discussed in the previous section, the pulses of concern are the time dependent transmitted and reflected pulses. For a homogeneously deforming sample, the amplitudes of these pulses are proportional to specimen strain rate and stress, respectively. Recall that specimen strain is simply calculated by integrating the strain rate. Though generating stress-time and strain-time diagrams is quite easy, they are not very useful. Therefore these time dependent pulses must somehow be combined to generate a dynamic stress-strain diagram, quite familiar to the engineer. One may suggest simply aligning the first temporal point of each diagram, second point, and so on. This is exactly correct, but determining the first point of each pulse is not a simple or precise task. Since the impact events are on the order of a few hundred microseconds, alignment of the stress and strain pulses becomes difficult. To the author's knowledge other investigators align these pulses based on the time it takes the pulses to travel in the bar and sample. This requires that the velocity in every different sample be known prior to testing. Further the pressure bar – specimen interfaces must be perfect for this timing scheme to work effectively. By applying certain numerical methods, these pulses can be aligned without relying on perfect interfaces and knowledge of sample wave velocities.

A major concern in longitudinal wave propagation is dispersion. Dispersion is a result of a bar's phase velocity dependence on frequency, which in effect distorts the wave as it propagates. Since it is the properties of the specimen we are after, the dispersive properties of the pressure bars need be known to accurately predict what the pressure pulses '*looked*' like at the pressure bar – specimen interfaces, not at the strain measurement locales. Most investigators use the numerical longitudinal wave velocities published by Bancroft [3]. Though his theory works well for predicting the dispersive nature of waves, other techniques specific to the actual apparatus used can offer improvements.

1.4 AREAS OF ADVANCEMENT

Two specific advancements in Hopkinson bar testing were eluded to in the previous section; Implementing numerical procedures to improve the alignment of pulses and experimentally ascertaining the dispersion relations for the actual bars used in the apparatus. The author has implemented a common numerical derivative algorithm to each of the strain histories. By means of identifying changes in slope, the appropriate pulses may be identified without any specific reference to time, nor prior knowledge of sample wave velocities, and no dependence on unknown interface effects.

The author has identified a technique by which the dispersive nature of bars can be determined experimentally. The resulting experimental dispersion relations are more appropriate for use in Hopkinson bar tests, since the relations are for the actual bars used, not a generic bar as is the case in theoretical dispersion relations.

A definite noise floor exists, near which signals can not be accurately recorded. By choosing a sample diameter based on the impedance mismatch between the sample and the pressure bar, the signal to noise ratio can be increased dramatically. As far as the author has been able to identify, no other investigators have attempted or at least documented attempts to optimize tests based on impedance mismatch. By doing so, the current author has been able to test low impedance materials at lower strain rates due to an increase in signal level.

By extending the rise time of the impact pulse, the distorting effects of dispersion can be dramatically reduced. A typical dispersion curve is shown in figure 1.2.

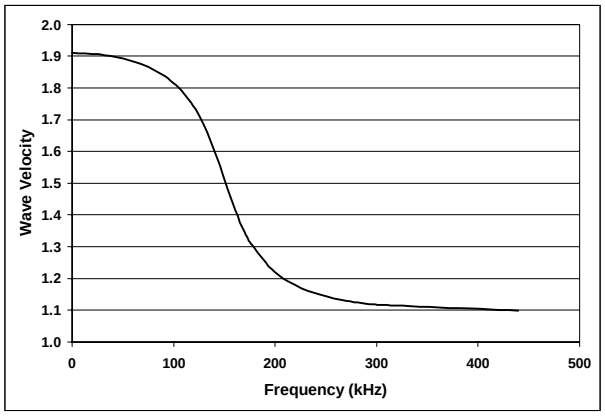

Figure 1.2 Typical dispersion curve for long rod

When a pulse's frequency content is comprised of many frequencies (i.e. wide bandwidth), the dispersive nature shown in figure 1.1 is at a maximum. As the bandwidth becomes narrower, the effects of dispersion are reduced to those shown in the specific range of frequencies comprising the pulse. The frequency makeup of a trapezoidal-shaped impact pulse is much less than that of a square-shaped impact pulse. This is due to the extended rise time of the trapezoidal-shaped pulse. To extend the rise time of an impact, small pieces of material need be placed between the striker bar and input bar. An investigation of this material size is presented.

1.5 TOPICS COVERED IN THESIS

Chapter Two is included as a review of the history of the split Hopkinson bar, as well as a review of other documents significant to this type of testing. Current areas of research are discussed.

Chapter Three introduces and fully develops the theory behind compressive split Hopkinson bar testing. This chapter begins by developing the one-dimensional equation of motion governing vibrations in a long, slender, elastic bar. Wave behavior is then described as a wave encounters various discontinuities including step changes in area and material. Herein the equations for calculating the specimen stress, strain,

and strain rate are derived. The justifications for all simplifying assumptions are pointed out explicitly. A means of correcting the dispersed strain pulses is presented, in the frequency domain, followed by a discussion of how to ascertain the actual dispersion curve for the pressure bars.

Chapter Four describes the Hopkinson bar setup at the naval laboratory in Dahlgren, Virginia. Descriptions of how to test materials under compressive loading and integrate the theoretical models into the data processing method are presented. The basis for choosing strain transducers, determining signal conditioner characteristics, and implementing numerical analysis procedures is shown.

The intent of the fifth chapter is to tie together the theory with the practice, as well as to present some experimental results. The author's insights towards improved testing procedures are given. Interpretations of the impedance equations derived in Chapter 3 are discussed in terms of sample diameter selection. A statistical analysis of copper is presented, that is applicable to all material types. Comparisons of the dynamic and static stress-strain characteristics of copper are shown.

The thesis is concluded in chapter six. Recommended areas of continual research are suggested. Some of these areas include the use of laser measurements in Hopkinson bar testing and changing pressure bar materials.

CHAPTER 2

BACKGROUND & LITERATURE REVIEW

2.1 INTRODUCTION

The present chapter is included as a chronological map of the development of the split Hopkinson bar apparatus. A time line approach is taken to summarize the major advancements leading to the current arrangement of the split Hopkinson bar apparatus, beginning with its founder. No single reference was found that attempts to or discusses completely the many technical aspects of split-Hopkinson-bar testing, so the author has attempted to glean the most significant advancements from various investigators and report them herein. The latter part of the chapter focuses on improvements towards data reduction techniques and testing procedures.

2.2 HISTORICAL PERSPECTIVE

1913 Bertram Hopkinson introduces a technique for determining the pressure – time relations due to an impact produced by a bullet or explosive. The key components of Hopkinson's apparatus were a means of developing impact like pressures, a long steel rod, a short steel billet, and a ballistic pendulum. By impacting one end of the rod, a compressive pressure wave of finite length is generated inside the rod. At the far end of the rod a short steel billet is attached, held by only a thin layer of grease. Hopkinson's idea was that as the compressive wave traversed down the bar, through the greased joint, and into the billet the wave would be reflected at the far end as a pulse of tension. Since the grease could not withstand any appreciable tensile loads, the billet would fly off with a definite momentum, measured with a ballistic pendulum. The time over which this momentum acts is the round trip time of the longitudinal wave in the billet. By running several tests of identical magnitude but different length cylindrical billets, as series of pressure – time curves were generated describing the impact event. Hopkinson was always capable of determining the maximum pressure and total duration of these impact events, but exact pressure-time curves were sketchy.

1941 Dennison Bancroft solves bar frequency equation of Pochhammer[XX] and Love[XX] for the velocities of longitudinal waves in cylindrical bars. Bancroft expressed the velocity of longitudinal waves in cylindrical bars in terms of a wave of infinite wavelength, Poisson's ratio, and the ratio of the bar diameter to the wavelength of interest. The usefulness of Bancroft's work – as applied towards Hopkinson bar testing – was not fully realized until much later when the computer sped up the data processing. Bancroft's work fueled significant advancements in the area of dispersion correction.

1948 Davies develops a technique using condensers to measure the strains existing in the pressure bar. The output from the condenser is proportional to the displacement–time relations that are proportional to the pressure-time relations assuming the pressures in the bars are under the elastic limit of the material. Using condensers to measure strains greatly improved the accuracy of Hopkinson's original apparatus, which relied on measuring the momentum of a steel billet flying off the end of the pressure bar. Recall that Hopkinson attached these billets with a film of grease, which introduced a major unknown related to the forces required to break the greased joint.

1949 Kolsky adds a second pressure bar to Hopkinson's original apparatus, hence the name *split* Hopkinson bar. Instead of attaching a billet at the far end of a bar, Kolsky sandwiched a specimen between the two bars. He presented expressions for calculating specimen properties based on strain histories in the bars. The strains were measured using similar condensers as those used by Davies. Of course the new two bar apparatus required measurements in both bars. This two bar technique has become the most widely used testing procedure today. In some literature the split Hopkinson bar may be referred to as the Kolsky bar.

1970 Hauser, et al, adds strain gages to the split Hopkinson bar to measure surface displacements.

2.3 CURRENT AREAS OF RESEARCH

The general theory governing Hopkinson bar testing has been well established for decades. In recent years investigators have taken up interests in the areas of data processing, experimental concerns, and employing different transducers to acquire data from the bars. This section is dedicated to reviewing the various areas of research significant to compressive Hopkinson bar testing. Some of the areas of research include effects of specimen geometry, experimentally ascertaining a bar's phase response, and the use of interferometers in measuring bar velocities.

As have many previous investigators, Woldesenbet and Vinson [4] performed tests to determine the effects of specimen geometry on testing results. Their experiments focused on varying the length-to-diameter ratio of the specimen from 0.5 to 2.0, but also included the use of square/rectangular specimens. In comparing the test results for various l/d ratios, 'no statistically significant effect of either l/d or geometry could be found.' Other investigators have suggested using l/d ratios in the range of 0.5 to 1.0 to minimize the errors due to pressure bar/specimen friction and radial inertia [5].

Gorham and Wu have made attempts to ascertain a bar's dispersive nature [6]. The dispersion correction they presented was based on bar phase characteristics determined by measuring the strains in a bar created from an impact of various sized metal spheres. Though this paper offers a valiant attempt to ascertaining the dispersive nature of bars, the study has a few shortcomings. By using only one measurement locale, the initial phase was assumed. In their method, the time pulses were shifted such that t=0 corresponded to the peak of the main pulse. This is done to remove the linear phase lag due to the output being measured at a time later than the impact occurs. Though the reason for time shifting the pulses is correct, simply aligning the peaks of the pulses does not yield the correct time delay. Other numerical

procedures, such as cross correlation or frequency domain analysis would lend more accurate results for determining the actual time delay responsible for the linear phase lag. The results of their work, though improved from past years, can be improved itself. The technique presented in this thesis does not rely on assuming an initial phase or removing the effects of the time delay. Other assumptions, as outlined in the thesis, are employed that must be considered when applying the author's technique for determining a bar's dispersive nature.

2.4 OTHER AREAS OF RESEARCH

This section, as its name suggests, is included for the purpose of literature consolidation. It by no means is attempting to summarize all of the work done concerning Hopkinson bar testing, but instead offers other interesting areas of research. Though the coverage is brief, most of the publications presented herein offer valuable insights and should therefore be examined in their entirety by anyone interested in Hopkinson bar testing.

In 1963, J. L. Chiddister, et al, introduced a technique for performing elevated temperature compression tests [7]. A few years later, in 1966, the use of the Hopkinson bar had been expanded to include the torsional loading of specimens [8]. It wasn't until 1968, however, that a convenient technique for performing tension tests was developed [9]. In 1991, the tensile Hopkinson bar test was further developed to allow pulse durations on the order of 500 μs [10]. A two dimensional analysis of the wave propagation in the split Hopkinson bar was presented by Bertholf, et al, in 1975 [11]. It was concluded that by correcting the one dimensional wave propagation model for lateral inertia, reasonable estimates of specimen properties could be attained.

CHAPTER 3

SPLIT HOPKINSON BAR THEORY

3.1 INTRODUCTION

This chapter introduces and fully develops the theory behind compressive split Hopkinson bar testing. It begins by developing the equation of motion for a rod in axial vibration, followed by theory governing longitudinal wave propagation. Both the complete and reduced equations are derived for calculating the specimen stress, strain, and strain rate. The phenomenon of wave dispersion is discussed. Corrections for the distorting effects of dispersion are modeled using two different techniques. The first uses the theoretical wave velocities presented by Bancroft, while the other is a new empirical dispersion correction. A summary is then included to discuss the equations used to calculate specimen properties. Underlying assumptions of split Hopkinson bar testing are discussed.

3.2 AXIAL VIBRATION OF BARS

The Hopkinson bar apparatus consists of two pressure bars of constant cross section A_o, elastic modulus E, and density ρ. Since the two bars are identical, it is only necessary to consider one of them in developing the equation of motion governing axial vibration. Typically the length-to-diameter ratio of the Hopkinson pressure bar is eighty or greater.

Many textbooks have been published that contain the derivation of the equation of motion for a uniform bar in axial vibration. All of the derivations begin by considering a differential cross section of a bar prior to deformation, then just after deformation begins. Figure 3.1 depicts the non-deformed pressure bar with differential element.

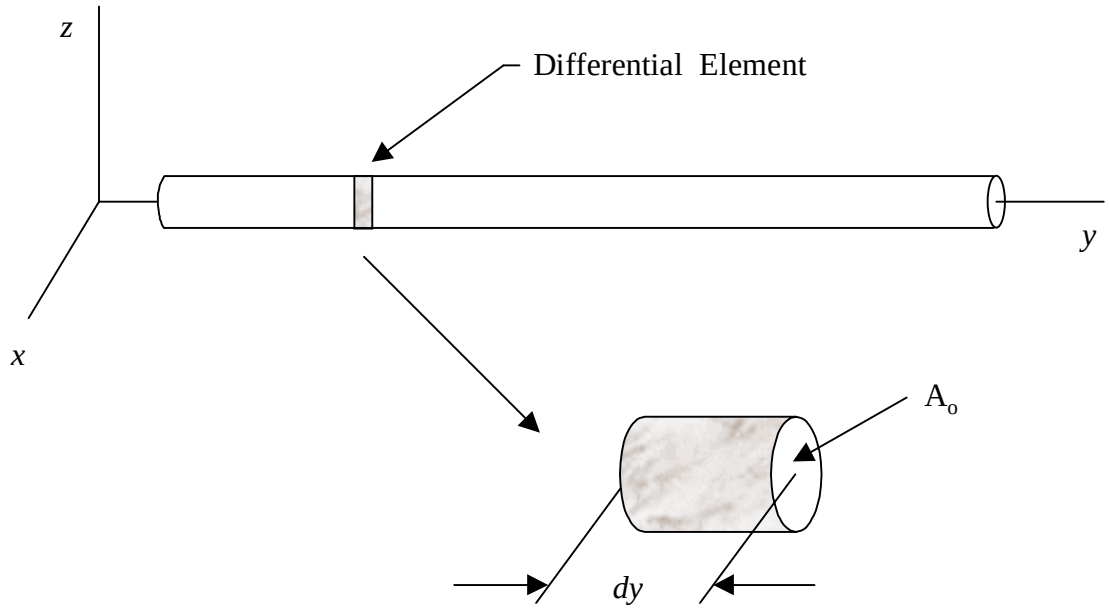

Figure 3.1 Pressure bar shown with differential element prior to deformation

The differential element has length *dy* and cross sectional area A_o. Prior to impact, the bar is in static equilibrium. Just after impact, particles in the differential element are in compression due to forces F_1 and F_2, as shown in figure 3.2.

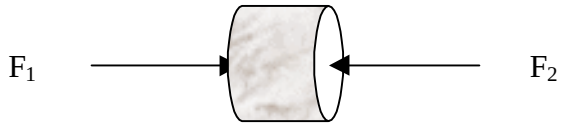

Figure 3.2 Differential element in compression

The forces in the differential element resisting compression are related to the stresses imposed on the cross section of that element. For elastic bars obeying Hooke's law, the stresses are related to the strains by the bar's elastic modulus. Further, these strains can be expressed in terms of the elemental displacements. Hence the forces generated to resist compression can be expressed in terms of the elemental displacements, *u*, as

$$F_Y = A_o E \frac{\partial u}{\partial y} \tag{3.1}$$

, assuming a uniaxial state of stress. The magnitude of this longitudinal force acts normal to the faces of the differential element as shown in figure 3.3.

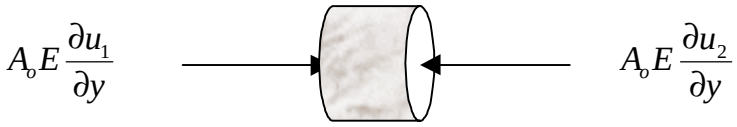

Figure 3.3 Forces resisting compression in differential element

By summing the forces acting on the element according to Newton's second law, $F = m\ddot{y}$, one arrives at the following equation describing the motion of the pressure pulses.

$$A_o E \frac{\partial u_1}{\partial y} - A_o E \frac{\partial u_2}{\partial y} = A_o dy \rho \frac{\partial^2 u_1}{\partial t^2} \tag{3.2}$$

This equation assumes that the particle acceleration is constant across the differential element. Simplifying the above equation yields the bar's equation of motion.

$$C_o^{\,2} \left[\frac{\partial u_1}{\partial y} - \frac{\partial u_2}{\partial y} \right] = \frac{\partial^2 u_1}{\partial t^2} dy \tag{3.3}$$

In equation 3.3, C_o is the wave velocity, calculated from

$$C_o = \sqrt{\frac{E}{\rho}} \tag{3.4}$$

,where E and ρ are the bars elastic modulus and mass density, respectively. Many investigators simplify the equation of motion by writing the displacements imposed on one side of the differential element in terms of the displacements of the other side, such that

$$u_2 = u_1 + \frac{\partial u_1}{\partial y} dy \tag{3.5}$$

This assumes that the rates of change of displacement of the two sides of the element are equal, which for a differential element is obviously reasonable. Upon differentiation this equation becomes

$$\frac{\partial u_2}{\partial y} = \frac{\partial u_1}{\partial y} + \frac{\partial^2 u_1}{\partial y^2} dy \tag{3.6}$$

By substituting the above equation into equation 3.3, the equation of motion for the bar reduces to

$$C_o{}^2 \frac{\partial^2 u_1}{\partial y^2} = \frac{\partial^2 u_1}{\partial t^2} \tag{3.7}$$

The equation of motion for the bar has no practical use in Hopkinson bar analysis, but does lend the theoretical wave velocity for a wave of infinite wavelength, which will be used later to calculate the specimen strain and strain-rate.

3.3 LONGITUDINAL WAVE PROPAGATION IN BARS

All bars have discontinuities that have significant effects on wave propagation. A few common discontinuities include a varying cross sectional diameter, an end, or a change in material (discussed as an impedance change.) For most Hopkinson bar applications the variation in cross section is generally a step change, usually occurring

at the pressure bar – specimen interfaces. The proper analyses for typical variations in cross section are derived in the following section.

3.3.1 REFLECTION FROM A FREE END

As no bar can be infinite, some type of termination for the ends of the bars always exists. Some common terminations in bars include a fixed end, a free end, or even a junction with another bar. As their names suggest, the fixed end occurs when the end of the bar is fixed to something and the free end occurs when the bar simply ends with nothing attached to it. Since the pressure bars have a free end, a brief discussion of the effect on wave propagation need be examined. A wave encountering a free end is reflected back into the median with characteristics related to the end condition. There are two important results from analyzing the free-end condition. At the free end of the bar, where the wave reflection occurs, the displacement doubles in value. Therefore any measurements of the pressure bar strains should be at a distance from the free ends. The other significant result of a free-end boundary condition is that the reflected wave is of opposite sign to the incident wave. So the initial compressive wave propagating in the pressure bar is reflected as a tensile wave. For further analyses of the free end condition, readers should refer to Graff [12].

3.3.2 STEP CHANGE IN CROSS SECTIONAL AREA & IMPEDANCE

The intent of this section is to describe the behavior of a wave as it encounters a discontinuity. The most commonly encountered discontinuities in split Hopkinson bar testing are step changes in cross sectional area and material properties. Waves encountering discontinuities are usually examined in terms of impedance. Impedance is defined as the ratio of the driving force to the velocity at a point in a structure (pressure bar in this case). Equation 3.8 is an expression for the mechanical impedance of the bars used in Hopkinson bar testing.

$$Z = \frac{F}{V} = s\rho C_o \tag{3.8}$$

The variables ρ, s, and C_o are the mass density, cross sectional area, and longitudinal wave velocity, respectively. The product ρc has a constant value for a given material; therefore it is often convenient for the two to be grouped together as one term. Notice that all of the impedance variables are physical properties; the impact event does not effect the impedance of the bars. Further notice that for any given bar material an impedance change can only occur by changing the cross sectional area.

Typically, discontinuities occur at the pressure bar – specimen interfaces. Since a wide range of materials may be under investigation, it is important to understand how waves respond to a change in median. Consider the familiar scenario in which one type of solid is sandwiched between two dissimilar solids of different cross sectional areas, depicted in figure 3.5.

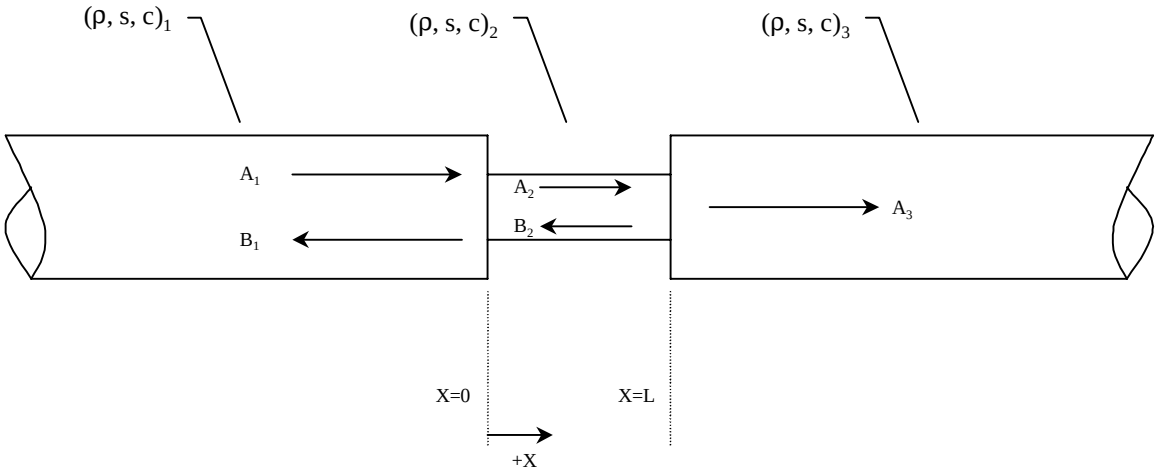

Figure 3.4 Schematic of step change in area and material properties

The variables ρ, s, and c are the same as those used in equation 3.8. The terms A_1-A_3 and B_1-B_2 denote the stress amplitudes for waves traveling to the right and to the left, respectively. At interface 1 (X=0), wave A_1 is partially reflected and transmitted as

waves B_1 and A_2, respectively. At interface 2 (X=L), wave A_2 is partially reflected and transmitted as waves B_2 and A_3, respectively. The level of reflection or transmission is dependent on the impedance mismatch at each interface. To quantify the stress amplitude variables and hence the amount a wave is reflected and transmitted at an interface requires an understanding of the dynamics at each interface. At each of the two pressure bar –specimen interfaces, the velocity of each material just to the left and right of the interface must be equal, since they are in intimate contact at all times. The forces just to the left and right of each interface must balance one another to satisfy equilibrium. By recognizing that these conditions must be true, equations describing the interface effects on wave propagation may be written. The system of equations for interfaces one and two are shown in Equations 3.9.1 and 3.9.2, respectively.

Interface 1 (X=0)

Continuity of Velocity

$$\frac{A_1 - B_1}{(\rho c)_1} = \frac{A_2}{(\rho c)_2}$$

Force Balance

$$s_1(A_1 + B_1) = s_2(A_2)$$

(3.9.1)

Interface 2 (X=L)

Continuity of Velocity

$$\frac{A_2 - B_2}{(\rho c)_2} = \frac{A_3}{(\rho c)_3}$$

Force Balance

$$s_2(A_2 + B_2) = s_3(A_3)$$

(3.9.2)

Notice from the four expressions that five stress variables exist, A_1, A_2, A_3, B_1, and B_2. To solve explicitly for any of these variables requires an additional expression containing the stress variables. Since no such expression exists, it becomes necessary at this point to define a couple of terms that allow the investigator to extract useful information from the equations.

By defining the transmission coefficient, a means of calculating the stress amplitude transmitted through a boundary exists. Subsequently expressed as α, the transmission coefficient is a number ranging in value from zero to one, zero representing a complete reflection and one representing 100% transmission (no reflection). The transmission coefficient is given by

$$\alpha = \frac{A_t}{A_i} \qquad \textbf{(3.10)}$$

The subscripts represent the transmitted and incident stress, respectively. The transmitted stress wave is in phase with the incident stress wave at the interfaces, therefore only the absolute magnitudes need be considered in equation 3.10.

Based on the conservation of energy principal, a conjugate term to the transmission coefficient may be defined as

$$\beta = 1 - \alpha \tag{3.11}$$

β, the reflection coefficient, is related to α by equation 3.11, since the wave either reflects or transmits at a boundary. As the name suggests, the reflection coefficient is a measure of the amount a wave is reflected at a boundary. With knowledge of one coefficient, the other can be calculated simply. The transmission and reflection coefficients can give an investigator valuable insight to properly testing a wide range of materials. With these coefficients defined, expressions describing wave transmission may be solved for at each boundary. The following expressions are for the fraction of a wave entering and leaving the sandwiched solid in figure 3.4, respectively.

$$\alpha_{12} = \frac{2s_1(\rho c)_2}{s_1(\rho c)_1 + s_2(\rho c)_2} \tag{3.12.1}$$

$$\alpha_{23} = \frac{2s_2(\rho c)_3}{s_2(\rho c)_2 + s_3(\rho c)_3} \tag{3.12.2}$$

By varying the cross sectional areas and ρc values in equations 3.12.1 and 3.12.2, many transmission coefficients can be achieved, perhaps some better suited than others.

3.4 CALCULATING THE SPECIMEN STRESS, STRAIN-RATE & STRAIN

The following section derives the expressions for calculating specimen stress, strain rate, and strain. Since the derivations are lengthy, a summary of the results has been

included at the end of the section. Also included in the summary, is a discussion of the assumptions employed in this theory.

3.4.1 SPECIMEN STRESS

The average stress in the specimen can be expressed in terms of the forces exerted on each surface of the specimen. A schematic representation of any specimen is shown in figure 3.5.

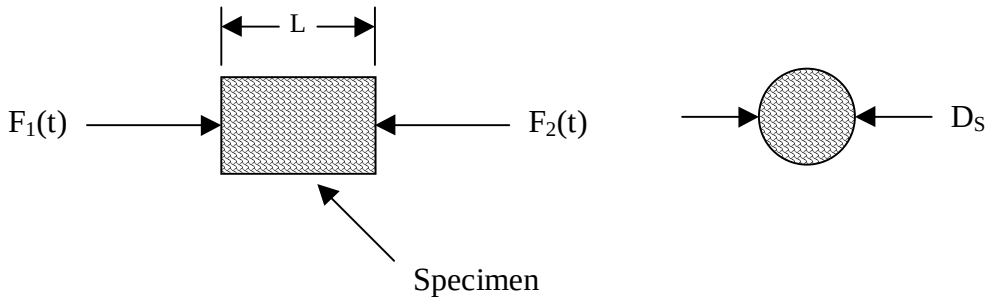

Figure 3.5 Schematic of cylindrical specimen

When the specimen is sandwiched between the pressure bars forces $F_1(t)$ and $F_2(t)$ exist on the specimen of instantaneous diameter D_S. The average force on the specimen is given by

$$F_{AVG}(t) = \frac{F_1(t) + F_2(t)}{2} \tag{3.13}$$

and hence the average stress on the cylindrical specimen is given by

$$\sigma_{AVG}(t) = \frac{F_{AVG}(t)}{\pi D_S^2 / 4} \tag{3.14}$$

The forces $F_1(t)$ and $F_2(t)$ acting at the specimen surfaces are due to the pressure bars. For a specimen in dynamic equilibrium, the forces at the ends of the pressure bars may be expressed in terms of the incident and reflected pressure bar strains as

$$F_1(t) = E[\varepsilon_I(t) + \varepsilon_R(t)]\frac{\pi D_{BAR}^2}{4} \quad \textbf{(3.15)}$$

$$F_2(t) = E\varepsilon_T(t)\frac{\pi D_{BAR}^2}{4} \quad \textbf{(3.16)}$$

where D_{BAR} is the diameter of the pressure bars. Substituting equations 3.13, 3.15, and 3.16 into equation 3.14 results in an expression for the average stress on the specimen in terms of the pressure bar strains

$$\sigma_{AVG}(t) = \frac{ED_{BAR}^2}{2D_S^2}[\varepsilon_I(t) + \varepsilon_R(t) + \varepsilon_T(t)] \quad \textbf{(3.17)}$$

If the specimen deforms uniformly, the strains in the incident bar are equal to the strain in the transmitter bar

$$\varepsilon_I(t) + \varepsilon_R(t) = \varepsilon_T(t) \quad \textbf{(3.18)}$$

and the expression for the average specimen stress can be reduced to

$$\sigma_{AVG}(t) = \frac{ED_{BAR}^2}{D_S^2}\varepsilon_T(t) \quad \textbf{(3.19)}$$

This equation shows that the specimen stress is proportional to the amplitude of the strain transmitted through the specimen into the transmitter bar.

3.4.2 SPECIMEN STRAIN-RATE AND STRAIN

The average strain rate is defined as the average strain divided by the time over which the straining occurs. Strain indicates displacement, which divided by time indicates velocity. The specimen strain rate may be calculated from the pressure bar - specimen interface velocities. These interface velocities can be calculated from the strains in the pressure bars. To derive the expressions for the specimen strain rate and strain in terms of the pressure bar strains, recall the equation of motion for the pressure bar, shown here for convenience.

$$C_o^{\,2}\frac{\partial^2 u_1}{\partial y^2}=\frac{\partial^2 u_1}{\partial t^2} \tag{3.7}$$

Recognizing that for harmonic waves $\frac{\partial^2 u_1}{\partial t^2}$ is equal to $\frac{\partial v}{\partial t}$, where v is the particle velocity, and that $E\frac{\partial}{\partial y}\left(\frac{\partial u_1}{\partial y}\right)=\frac{\partial p}{\partial y}$, where p is the stress across the cross section, the equation of motion can be rewritten in terms of the pressure and velocity across the bar cross section as

$$-\frac{\partial p(y,t)}{\partial y}=\rho\frac{\partial v}{\partial t} \tag{3.20}$$

Notice from equation 3.20 that to solve for the particle velocity in a bar requires knowledge of the pressure in the bar. If we assume a positive traveling harmonic wave of the form

$$p(y,t)=Pe^{i(\omega t-ky)} \tag{3.21}$$

where P is the amplitude of the pressure, ω is the frequency, t is the time, k is the wave number and is defined as $k=\frac{\omega}{C_o}$, and y is the spatial location of the wave an

expression for the instantaneous particle velocity can be derived. Taking the first derivative of equation 3.21 with respect to y, one arrives at

$$\frac{\partial p(y,t)}{\partial y} = -ikPe^{i(\omega t - ky)} \tag{3.22}$$

Substituting this derivative into equation 3.23 and pre-multiplying the RHS of equation 3.7 by the heavyside operator, one attains

$$ikPe^{i(\omega t - ky)} = \rho i\omega v(y,t) \tag{3.23}$$

Which can be solved for the particle velocity, given by equation 3.24.

$$v(y,t) = \frac{k}{\rho\omega} Pe^{i(\omega t - ky)} \tag{3.24}$$

Substituting the expression for *k* and *p(y,t)* back into the expression for the particle velocity yields

$$v(y,t) = \frac{1}{\rho C_o} p(y,t) \tag{3.25}$$

where *P* is the pressure across the cross section. For a uniaxial state of stress, the pressure is equal to the stress over the pressure bar cross section. Therefore, *p(y,t)* can be written in terms of the bar strain as

$$p(y,t) = \varepsilon(y,t)E \tag{3.26}$$

By substituting equation 3.26 into equation 3.25 yields an expression for the particle velocity in terms of the bar strain as

$$v(y,t) = C_o\varepsilon(y,t) \tag{3.27}$$

For a negative traveling wave the particle velocity is expression by

$$v(y,t) = -C_o \varepsilon(y,t) \tag{3.28}$$

With expressions for the particle velocity in terms of the pressure bar strains, specimen strain rate can be calculated rather simply. The average strain rate at any given time is given by

$$\frac{d\varepsilon}{dt} = \frac{v_{\text{int}erface2} - v_{\text{int}erface1}}{L} \tag{3.29}$$

The velocity at interface 1 is comprised of the incident (+ traveling wave) and the reflected (- traveling wave) as

$$v_{\text{int}erface1} = C_o \varepsilon_I - C_o \varepsilon_R = C_o(\varepsilon_I - \varepsilon_R) \tag{3.30}$$

To calculate the velocity of the second interface only requires knowledge of the strain transmitted into the pressure bar. Since the transmitted wave propagates in the positive direction, the velocity of interface two appears as a positive quantity in equation 3.31.

$$v_{\text{int}erface2} = C_o \varepsilon_T \tag{3.31}$$

By substituting these interface velocities into the expression for the specimen strain rate yields an expression for the specimen strain rate in terms of the pressure bar strains as

$$\frac{d\varepsilon_s}{dt} = -\frac{C_o(\varepsilon_T - \varepsilon_I + \varepsilon_R)}{L} \tag{3.32}$$

where the negative sign represents compression. If the specimen deforms uniformly such that

$$\varepsilon_I(t) + \varepsilon_R(t) = \varepsilon_T(t) \tag{3.33}$$

The expression for the specimen strain rate can be reduced to

$$\frac{d\varepsilon_s}{dt} = -\frac{2C_o}{L}\varepsilon_{reflected} \tag{3.34}$$

which can be integrated to yield the specimen strain

$$\varepsilon_s(t) = -\frac{2C_o}{L}\int \varepsilon_R(t)dt \tag{3.35}$$

Though a bit lengthy to arrive at, the equations for calculating specimen properties are rather simple to use. A review of the equations used through out the remainder of the thesis is presented in the following section.

3.4.3 SUMMARY OF STRESS, STRAIN, AND STRAIN RATE EQUATIONS

For a uniformly deforming specimen, the expressions relating pressure bar strains to specimen properties are greatly reduced. Before discussing the implementation of these expressions, an overview of the physics behind the test is necessary. After the striker bar impacts the input bar, an elastic compressive wave is generated that propagates towards the specimen. Upon reaching the specimen, part of the wave is reflected while the remainder is transmitted through the specimen and into the output bar. By mounting strain transducers to the surfaces of the pressure bars, the reflected and transmitted waves can be recorded for use in equations 3.36.

$$\frac{d\varepsilon_s(t)}{dt} = -\frac{2C_o}{L}\varepsilon_R(t)$$

$$\varepsilon_s(t) = -\frac{2C_o}{L}\int_0^t \varepsilon_R(t)dt \qquad \textbf{(3.36)}$$

$$\sigma_s(t) = E\frac{A_o}{A}\varepsilon_T(t)$$

The recorded strain histories must first be corrected for dispersion, then examined such that the precise beginning and ending of the reflected and transmitted pulses may be identified. Many testing conditions greatly affect the implementation and effectiveness of equations 3.36. For instance the length of the impact pulse determines how much the specimen may be deformed. As mentioned the waves are dispersed, which in effect smears the waveforms. The fundamental assumption that the specimen deforms uniformly must be enforced by lubricating the specimen – pressure bar interfaces and choosing appropriate specimen dimensions. By carefully addressing these issues, dynamic stress-strain relations can be found for a broad range of materials using equations 3.36.

3.5 IMPACT OF TWO COLLINEAR RODS

Recall that under certain circumstances, specimen strain rate is proportional to the amplitude of the reflected pulse. Since most investigators are interested in materials sensitivity to changing strain rate, testing materials at a constant strain rate is desirable. Thus it would seem to achieve a constant strain rate test would require a constant magnitude reflected pulse. The stress pulses in the Hopkinson Bar apparatus are usually generated by firing a shorter bar of similar material into the first pressure bar. To avoid reinventing the wheel, prior analyses for the collinear impact of two bars have been reviewed. Graff presented the most pertinent study of collinear impact applicable to Hopkinson bar testing [13], and is what has been referenced herein. Should other types of impact analyses be desired, his book is an excellent resource.

The perfect impact of similar bars results in a square shaped pulse of magnitude $\sigma = V_1 \rho_1 C_o / 2$ and of duration $T = 2l_1 / C_o$. The parameters V_1, ρ_1, C_o, and l_1 are the impact bar's velocity just before impact, density, wave velocity, and length, respectively. These equations suggest that for a given impact bar, the stress generated is proportional to its impact velocity and its duration is only related to physical properties of the impact bar. The stress is always a step change. Unfortunately, distorting wave phenomenon render the utility of a square pulse very limited. The following section fully discusses the phenomenon of dispersion, and its distorting effects on wave shape.

3.6 PRESSURE WAVE DISPERSION

In section 3.2 the development of the equation of motion was presented. In its development, the effects of lateral inertia were not included for the sake of simplicity. By ignoring the effects of lateral inertia, the dispersive nature of wave propagation in bars can not be described. The derivation of the wave equation including lateral inertia effects results in a system whose propagation velocity has a functional relationship to frequency. The dispersive nature of rods was first pointed out by Pochhammer [14]. It was Love [15] who later presented the development of the frequency dependent wave equation. It was found that for wavelengths on the order of the pressure bar diameter, longitudinal waves are dispersive. Dispersion is a direct result of the wave propagation velocity dependency on wavelength. In 1948, Davies [16] performed experiments confirming that the aforementioned lateral inertia terms do indeed account for the oscillations in the time domain. Hence the author has chosen to use the numerical solutions, offered by Bancroft, to the frequency equation for longitudinal wave velocity in cylindrical bars. Bancroft presented, in tabular form, the velocity of longitudinal waves in terms of the velocity of a wave of infinite wavelength and the variables: Poisson's ratio, and the ratio of the bar diameter to the wavelength. The result of Bancroft's work for various bar materials is shown in figure 3.6.

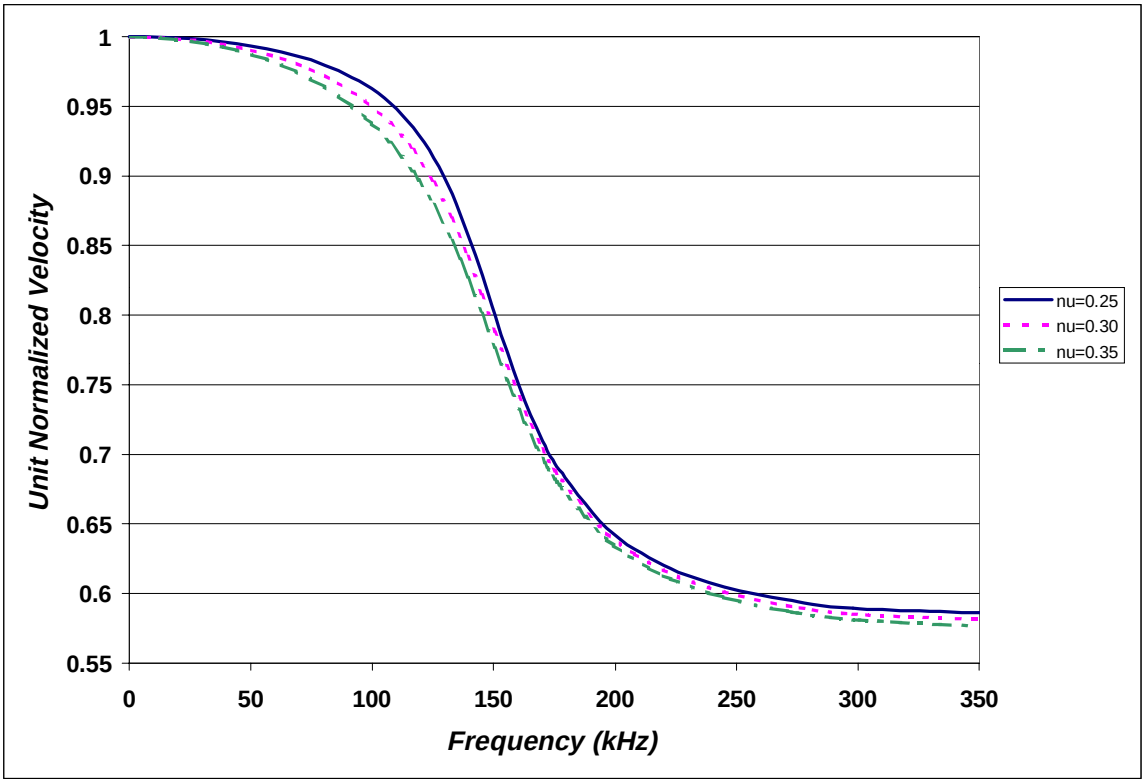

Figure 3.6 Unit normalized velocity in ¾" bar of various Poisson ratios

The effects of this dispersion manifest themselves as oscillations in the time-domain signal. Take for instance the trapezoidal shaped wave in figure 3.7.

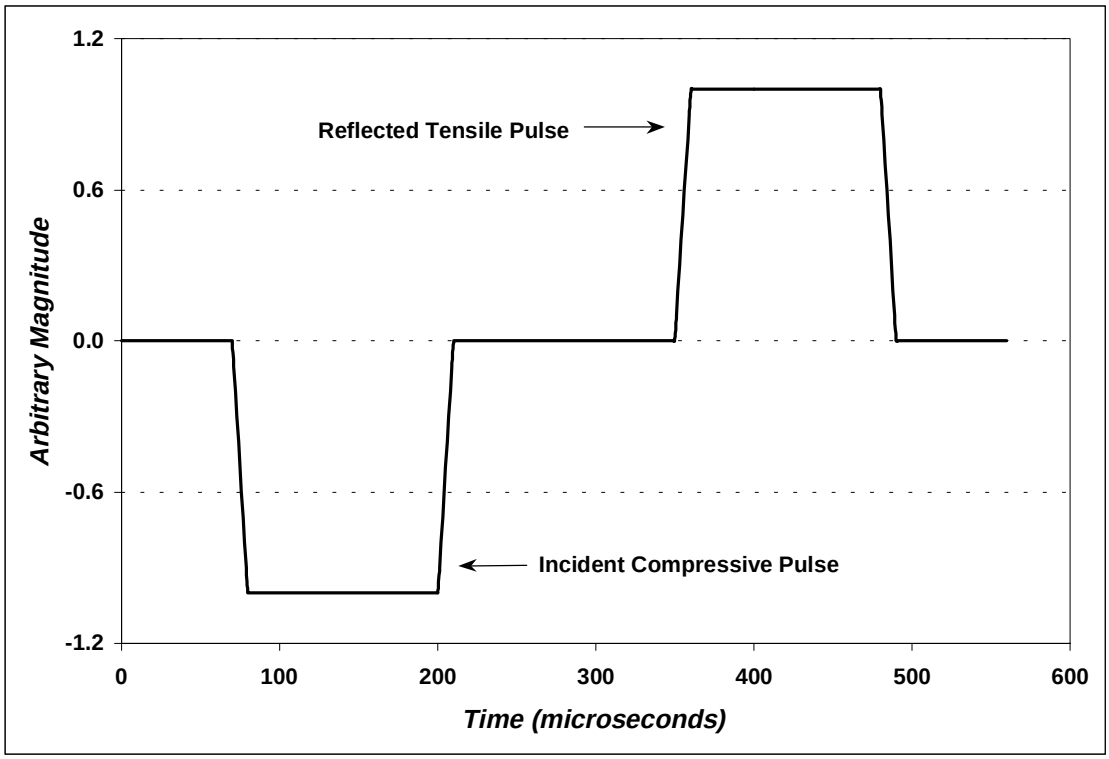

Figure 3.7 Trapezoidal wave typical of Hopkinson bar strain history

With no dispersion, the strain history of a wave traveling in a bar is comprised of the incident compressive pulse and it's reflection, unchanged in form only sign. Upon examination of the Fast Fourier Transform of this strain history (figure 3.8), frequency components can be found spread over the entire range of gross dispersion identified in figure 3.6.

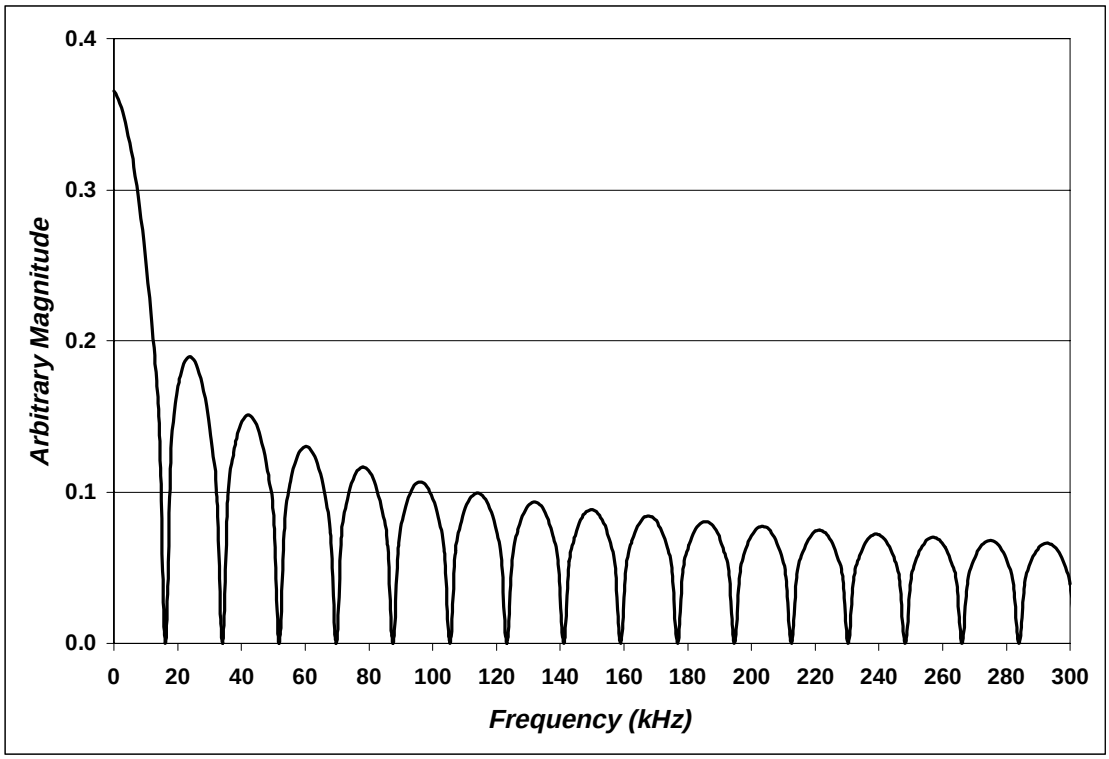

Figure 3.8 Fast Fourier Transform of trapezoidal pulse

These individual frequencies each travel with different velocities. Therefore the waveform in figure 3.7 can not remain unchanged in form after traversing along the bar. By accounting for thirty inches of dispersion in a ¾" steel bar, the trapezoidal waveform of figure 3.7 becomes distorted as shown in figure 3.9.

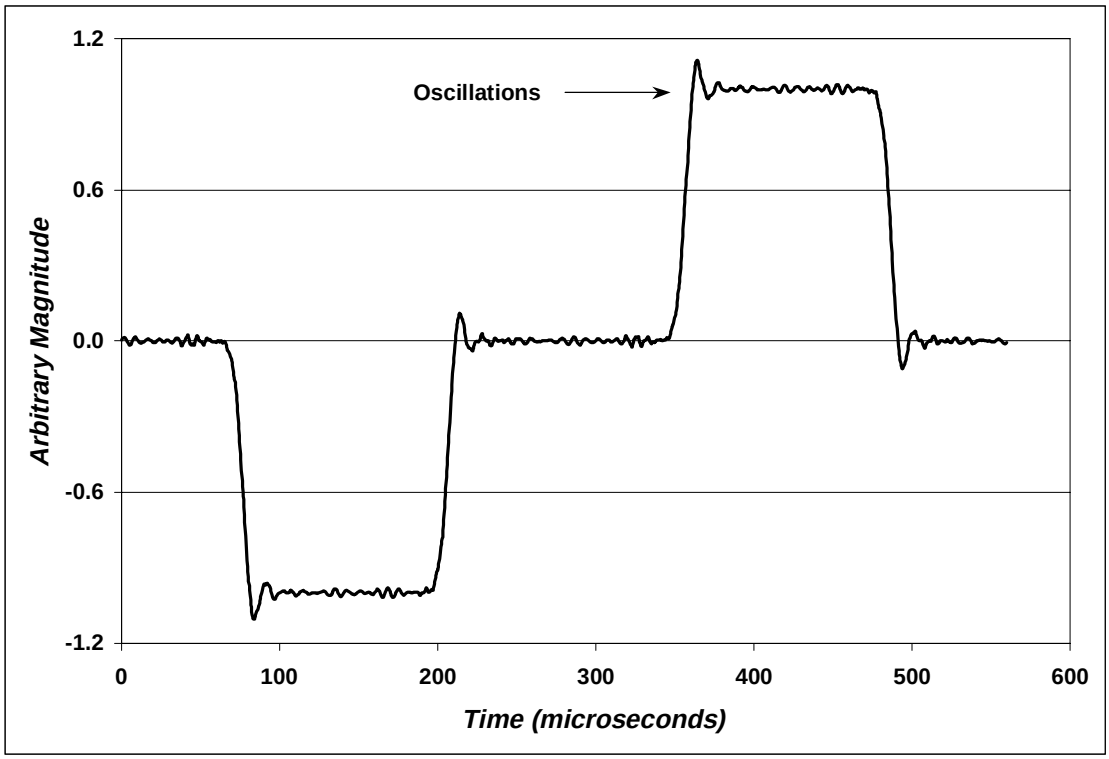

Figure 3.9 Trapezoidal pulse with 30" of dispersion in ¾" bar

Notice that the distortion appears as large oscillations overlying the general trapezoidal shape. The frequency range of the pulse affects the magnitudes of these oscillations. For pulses with a small frequency bandwidth, the oscillations are minimal. However, pulses with wideband frequency content have large oscillations. As a direct comparison of the non-dispersed and dispersed trapezoidal waveforms, the pulses have been overlaid in figure 3.10.

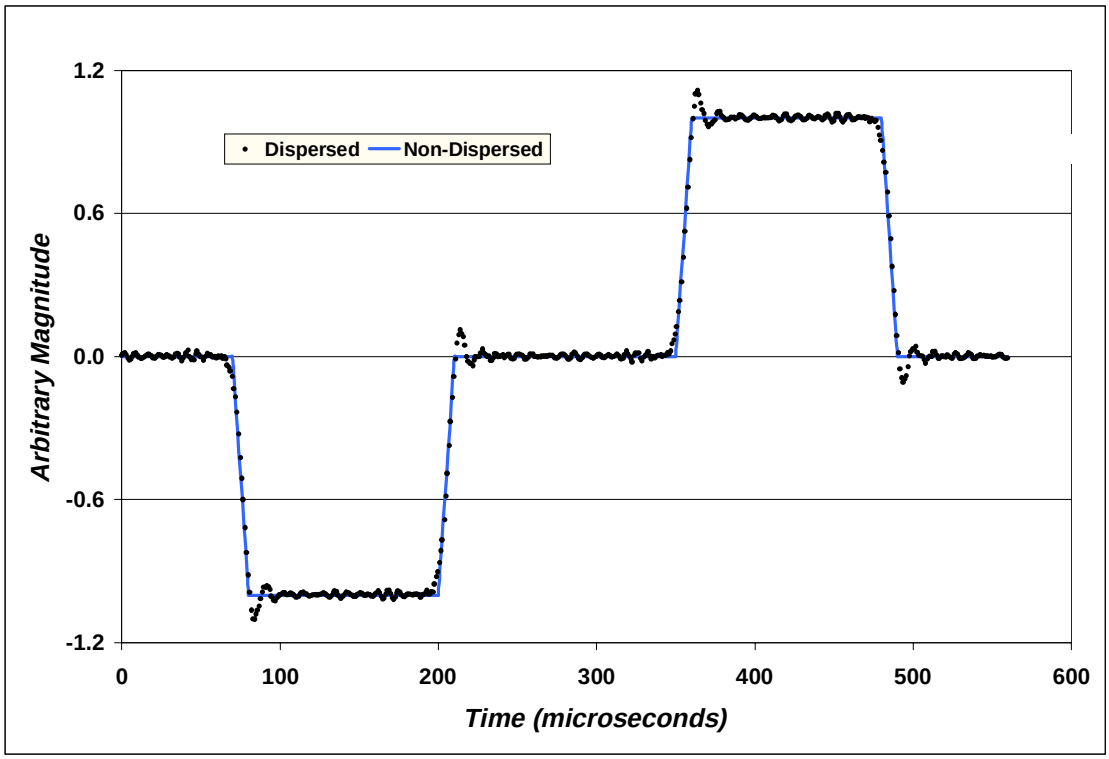

Figure 3.10 Overlayment of dispersed and non-dispersed trapezoidal pulses

Clearly, in the time-domain dispersion can be recognized by oscillations in the waveform. In the frequency domain, however, wave dispersion can be described by a shift in phase for each spectral component. By adjusting individual frequency components, the effects of dispersion can theoretically be 100% accounted for. Using a Fourier transformation of the strain pulse permits access and hence adjustment of phase values. A discussion of a technique for performing appropriate phase adjustments is discussed in the following section.

3.6.1 THEORETICAL DISPERSION CORRECTION

Typically the strain histories are recorded in the middle section of the pressure bar, allowing for the separation of the incident and reflected pulses. The equations presented in previous sections related to specimen properties require knowledge of the strain histories at the pressure bar – specimen interfaces. To predict what the strain

pulses 'looked' like at the pressure bar - specimen interfaces requires substantial data manipulation. The most convenient means of manipulating this data is by transforming the time-domain strain signals into the frequency domain, then applying appropriate phase shifts to each spectral component to compensate for the bar dispersion, then transforming the corrected frequency domain strain pulses back into the time-domain.

With knowledge of the wave velocities for a pressure bar, one can correct for the distorting effects of dispersion in the frequency domain. Any periodic wave can be described by superimposing a number of harmonic waves of different frequency. A lengthy discussion of Fourier transforms is not intended; hence only main ideas are presented. The general form of the Fourier transform is shown in equation 3.37.

$$F(t) = \frac{1}{N}\sum_{n=1}^{N}\left[A_n \cos(2\pi f \cdot nt) + B_n \sin(2\pi f \cdot nt)\right] \qquad \textbf{(3.37)}$$

Where the variables N, f, n, and t are the total number of data points, frequency resolution, temporal index, and time, respectively. The constants A_n and B_n are the magnitudes of the real and imaginary components, respectively. To correct for dispersion each spectral component must be phase shifted to compensate for the varying wave velocity. By adjusting equation 3.37 as follows, the effects of wave dispersion can be removed from the waveforms.

$$F_{corrected}(t) = \frac{1}{N}\sum_{n=1}^{N}\left[A_n \cos(2\pi f \cdot nt + \phi) + B_n \sin(2\pi f \cdot nt + \phi)\right] \qquad \textbf{(3.38)}$$

$$\begin{aligned} \phi &= \phi_o - \phi_n, \\ &= 2\pi \cdot y \cdot \left(\frac{1}{\lambda_o} - \frac{1}{\lambda_n}\right), \\ &= 2\pi f \cdot n\left(\frac{1}{C_o} - \frac{1}{C_n}\right) y \end{aligned} \qquad \textbf{(3.39)}$$

where ϕ accounts for the phase lag of the higher frequencies components traversing away from the pressure bar – specimen interfaces. C_o is the infinite wavelength wave velocity and C_n is the wave velocity for each particular frequency given by the FFT. λ_x is the wavelength given by C_x/f. The constant y is the distance the wave traversed before being recorded. Before calculating the phase lag, investigators have a choice to make concerning the wave velocities C_n. Either theoretical wave velocities or experimentally determined wave velocities can be used. Techniques are developed in the following section that allow the determination of wave velocities for individual pressure bars.

3.7 EXPERIMENTAL DISPERSION CORRECTION

In lieu of using the tabulated wave velocities presented by Bancroft to satisfy equation 3.39, actual wave velocities can be determined for each of the pressure bars in the Hopkinson apparatus. By solving equation 3.39 for C_n, shown in equation 3.40, one can ascertain the bar phase velocity characteristics.

$$C_n = \frac{2\pi \cdot n\omega \cdot y \cdot C_o}{2\pi \cdot n\omega \cdot y - C_o \Phi} \qquad \textbf{(3.40)}$$

The constants y and C_o can be determined relatively easily, the former simply measured with a standard tape measure. To calculate C_o, the investigator simply needs to examine the strain history generated by an impact. By identifying the leading edges of the incident and reflected pulses and knowing how far the strain gage is from the reflection end of the bar, the low frequency wave velocity may be calculated. To determine Φ, the dispersed phase, requires that an impact be generated, traversed, and recorded in the pressure bars. This must be done in a particular way, outlined just below.

Ascertaining the dispersive nature of the input bar requires that a strain history be recorded in the output bar in two different experiments. The output bar must be positioned such that the striker bar impacts it directly, as shown in figure 3.11.

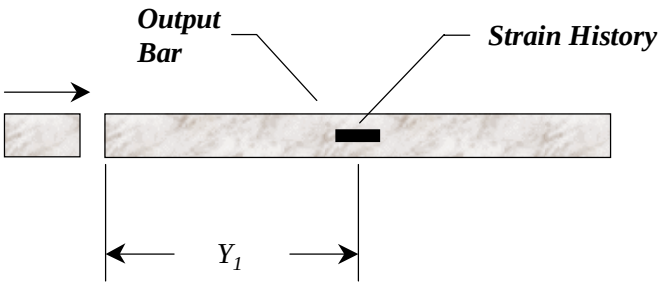

Figure 3.11 First experiment to perform on output bar

After recording the stress pulse generated from the impact, the output bar must be moved back to its traditional location, with the leading end pressed against the trailing end of the input bar. The striker bar must then be propelled into the input bar, in which the stress wave will traverse before entering the output bar, where the strain history is again recorded. Figure 3.12 illustrates the second experiment necessary for the calculation of the input bar's dispersive nature.

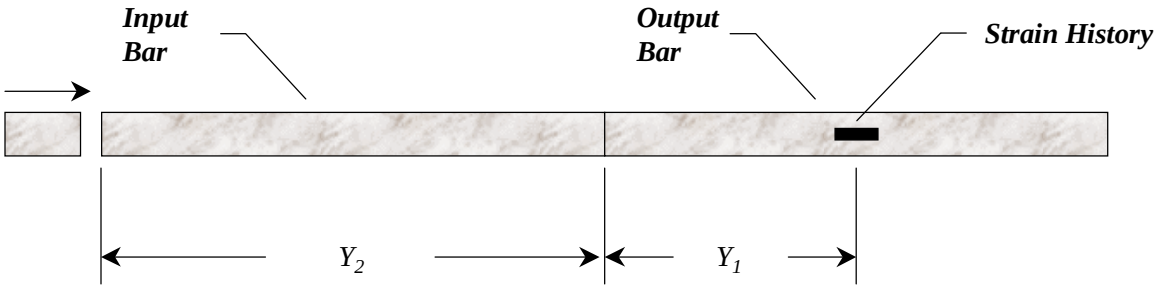

Figure 3.12 Second experiment to perform on output bar

The stress pulse disperses over distance Y_1, before being recorded in the first experiment. In the second experiment, the stress pulse disperses Y_1 plus the length of the input bar, Y_2. The difference in phase between the two strain histories is the

dispersed phase over a distance $Y_1 + Y_2$. Substitution of this phase into equation 3.40 facilitates the calculation of the wave velocities in the input pressure bar. A similar procedure may be followed to characterize the dispersive nature of the output bar.

In the second experiment, it is assumed that the interface has negligible effect on wave propagation. Applying a thin layer of grease between the two pressure bars minimizes the interface effects, as no reflected wave is generated. Also, care should be taken that sufficient energy is supplied at desired frequencies during impact. It may be necessary to use several different impact bars to achieve adequate frequency extension.

With a strong grasp on the theory behind Hopkinson bar testing, informed decisions concerning the apparatus can be made. The Hopkinson bar apparatus is discussed in the following chapter.

CHAPTER 4

EXPERIMENTAL TEST SETUP

4.1 INTRODUCTION

This chapter presents a typical experimental setup for the compressive split Hopkinson bar test. The basis for choosing strain transducers, signal conditioner characteristics, data sampling rate, and numerical analysis procedures are described. Various testing concerns, data acquisition, and data reduction techniques are discussed. The basic procedure to performing tests is described.

4.2 SPLIT HOPKINSON BAR APPARATUS

All compressive split Hopkinson pressure bar (SHPB) apparatuses have the same general components. They include an impact bar usually propelled by a gas chamber, an incident bar and transmitter bar, strain transducers with signal conditioners, and a means of digital storage. A schematic of the SHPB is shown in figure 4.1.

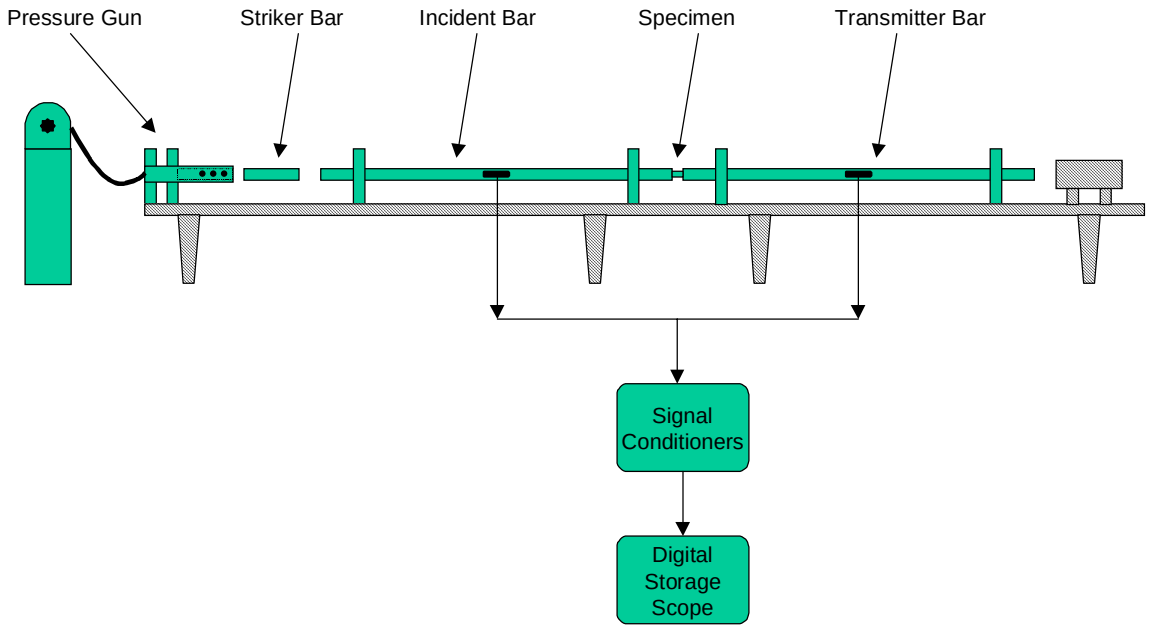

Figure 4.1 Typical compressive split Hopkinson bar apparatus

The following photographs are of the Hopkinson bar apparatus used at NSWCDD's facility. Figure 4.2 is the apparatus as viewed from the pressure gun end.

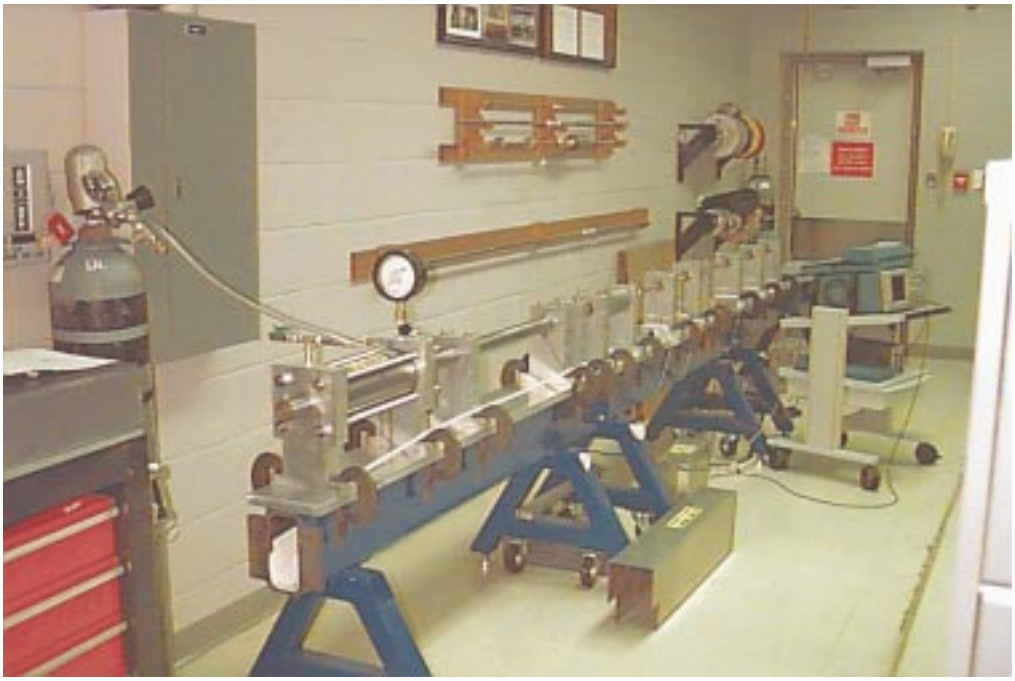

Figure 4.2 Apparatus as viewed from striker bar end

A view from the end of the transmitter bar better shows the length of the pressure bars. From beginning to end the apparatus is over fifteen feet long.

Figure 4.3 Apparatus as viewed from transmitter bar end

A close up photo of the gas gun is shown in figure 4.4. The holes drilled into the end of the barrel vent the pressure behind the striker bar, allowing the striker bar to exit.

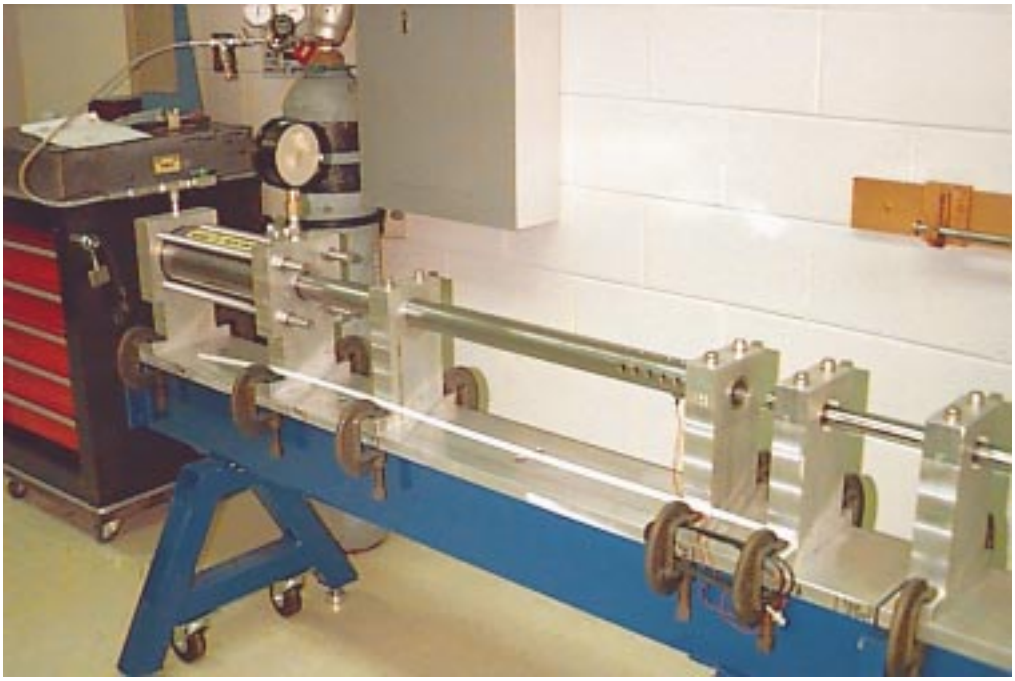

Figure 4.4 A view of the gas gun and striker bar mechanism

The pressure bars are usually made of high strength elastic material, such as maraging steel. Several collars support the pressure bars, allowing it to slide freely and to remove any bending waves due to an impact. Transducers mounted to the pressure bars respond to the instantaneous strain. Once amplified, a digital storage oscilloscope records these strain signals. Many factors influence the appropriate selection of the various components in the SHPB test.

4.2.1 DESIRABLE PRESSURE BAR CHARACTERISTICS

It is the yield strength of the incident pressure bar that limits the maximum attainable specimen stress, since the equations developed in chapter 3 are valid only for an elastic bar. Before choosing a pressure bar material, careful consideration must be given to the desired sample stress levels. The pressure bars used in NSWCDD's apparatus are Vascomax C-350 centerless ground MIL-S-46850D, with properties shown in table 4.1.

Table 4.1 Properties of NSWCDD's pressure bar material

Mechanical Properties	
Tensile Strength	370 ksi
Yield Strength	350 ksi
Reduction of Area	34.0 %
Elongation	6.0 %
Charpy Impact Test	6.0 ft/lbs

To achieve very high strain rates requires reducing the bar's cross sectional area, and consequentially diameter. It is often desirable to have several different pressure bars; each suited for testing materials in a certain range of strain rate and strain. Choosing an appropriate length for the bars requires that two conditions be met:

- Length-to-diameter ratio meets requirements for one-dimensional propagation theory
- Length of bar is at least twice that of the compressive pulse generated during impact

Most texts suggest that the bar have a length-to-diameter ratio of at least ten. The length of the pressure bar affects how much strain a specimen may see, since strain is related to the total pulse duration, which is directly related to the length of the pressure bar. To measure the incident and reflected pulses independently requires that the bar length exceed twice the length of the impact pulse. Typically pressure bars are 60 inches or greater.

4.2.2 ENFORCING ONE DIMENSIONAL WAVE THEORY

In chapter three, wave theory was developed for a one-dimensional pressure wave propagating axially in a slender elastic rod. It is assumed for all calculations in this thesis that one-dimensional theory applies. Geometry plays a major role in determining whether a wavefront can be described by one variable or not. As was presented in the previous section, the bar length-to-diameter ratio needs to be greater than ten. The most important experimental factor influencing the nature of wave propagation is bar alignment. If the striker bar impacts the incident bar at an angle, a non-uniform wave distribution will exist across the bar cross section, and hence a multi-dimensional strain field will result. This also holds true for the alignment of the incident bar with the transmitter bar. By carefully aligning the striker bar with the incident bar such that the two remain in the same plane, a one-dimensional wavefront can be attained experimentally.

4.3 TESTING CONCERNS

Recall from chapter three that the equations leading to specimen stress, strain rate and strain were greatly reduced by assuming that the specimen deforms uniformly over its length. Many investigators have been concerned with this assumption and have dedicated lengthy studies to it. This section describes problems with assuming that the specimen deforms uniformly, and how most investigators circumvent these problems. During the compression test the specimen shortens and expands. At the pressure bar – specimen interface a frictional constraint exists due to this radial expansion. The frictional effects are highest when the specimen is at rest, then reduce once the static friction is broken and the specimen starts sliding. If the ends are restrained in the beginning of the test, the middle section of the specimen must deform. This results in a barrel shaped specimen, clearly not uniform. By applying a thin film of lubricant at the interfaces, this frictional constrain can be greatly reduced. Table 4.2 is a list of static and dynamic friction coefficients, reproduced from CRC's Handbook of Tables for Applied Engineering Science [17].

Table 4.2 Coefficients of static and sliding friction

Materials	***Static***		***Sliding***	
	Dry	***Greasy***	***Dry***	***Greasy***
Hard steel on hard steel	*0.78*	*0.0052-0.23*	*0.42*	*0.029-0.12*
Mild steel on mild steel	*0.74*	*NV*	*0.57*	*0.09-.019*
Aluminum on mild steel	*0.61*	*NV*	*0.47*	*NV*
Teflon on steel	*.04*	*NV*	*NV*	*.04*
Tungsten carbide on steel	*0.5*	*0.08*	*NV*	*NV*
			NV : no value given	

By lubricating the interfaces between the specimen and the pressure bars, uniform deformation conditions exist much sooner in the test than without lubricant.

Specimen diameters are smaller than the pressure bar diameters, since the sample expands during the test. It is important to align the centerlines of the sample and pressure bars to load the transmitter bar uniformly. Benny Simpson, of NSWCDD,

designed and built a clever device for centering the sample on the pressure bar. The user simply slides the alignment tool over the end of the pressure bar, followed by placing the sample into the alignment tool, as shown in figure 4.5.

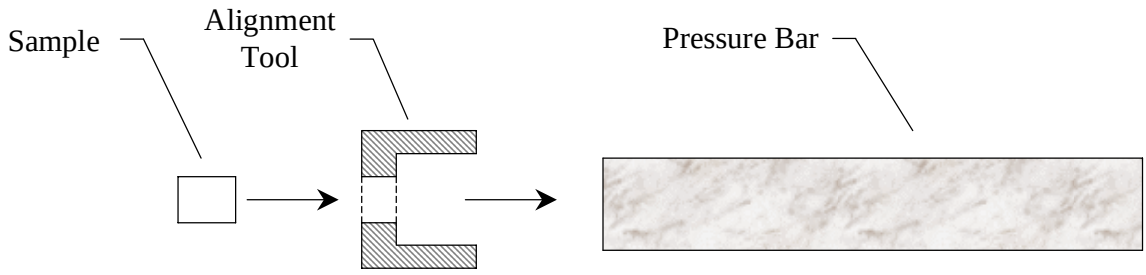

Figure 4.5 Technique for aligning sample with pressure bars

The thin layer of lubricant on the end of the sample is enough to hold the sample in place, while the user removes the alignment tool and slides the other pressure bar against the opposite sample end.

4.4 DATA ACQUISITION AND INSTRUMENTATION

Much emphasis has been placed on attaining one-dimensional wave propagation. This is because the induced stresses and strains are constant throughout the bar's cross section. From a measurement standpoint, this is extremely important since surface measurements on the pressure bars will fully describe the instantaneous elastic strains in the bars. Anyone in question of this importance can try measuring a non-uniform wave distribution inside a solid bar. Since the pressure wave is of dynamic nature – typical rise times of 10-30 μs - transducer properties such as frequency response and rise time become a primary concern. To identify appropriate transducer specifications, the dynamics of the pressure wave must be closely examined.

4.4.1 THE ELECTRICAL RESISTANCE STRAIN GAGE

The most common type of strain transducer is the electrical resistance strain gage. These are extremely versatile due to their small size and ease of installation. For the purposes of pressure bar measurements, a single element strain gage can be used. A diagram of the single element strain gage with dimensions is shown in figure 4.6.

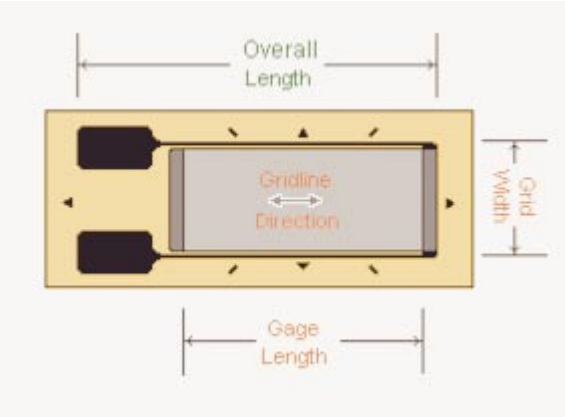

Figure 4.6 Uniaxial strain gage (*from Measurements Group Inc.*)

When the gage deforms, an electrical output is produced that is directly proportional to the strain across the length of the gage's element. There are at least three significant considerations when using strain gages for measuring dynamic signals. The following limitations should be understood before choosing a strain gage, and especially before interpreting dynamic strain data:

- Frequency resolution is lost for wavelengths near that of the gage length
- Spatial resolution is a concern for pulses on the order of the gage length
- The ability of a gage to 'track' a signal, or rise time, must be known

The ability to resolve a wave spatially becomes limited for pulses on the order of the gage length. As the gage length increases, so too does the ability to resolve spatial

location. Therefore the total length of the pulse of concern must be much greater than the gage length.

The output of a strain gage tends to give an integrated average of the strains imposed over its gage length. Consider the three different wavelengths and three different gage lengths, shown in figure 4.7.

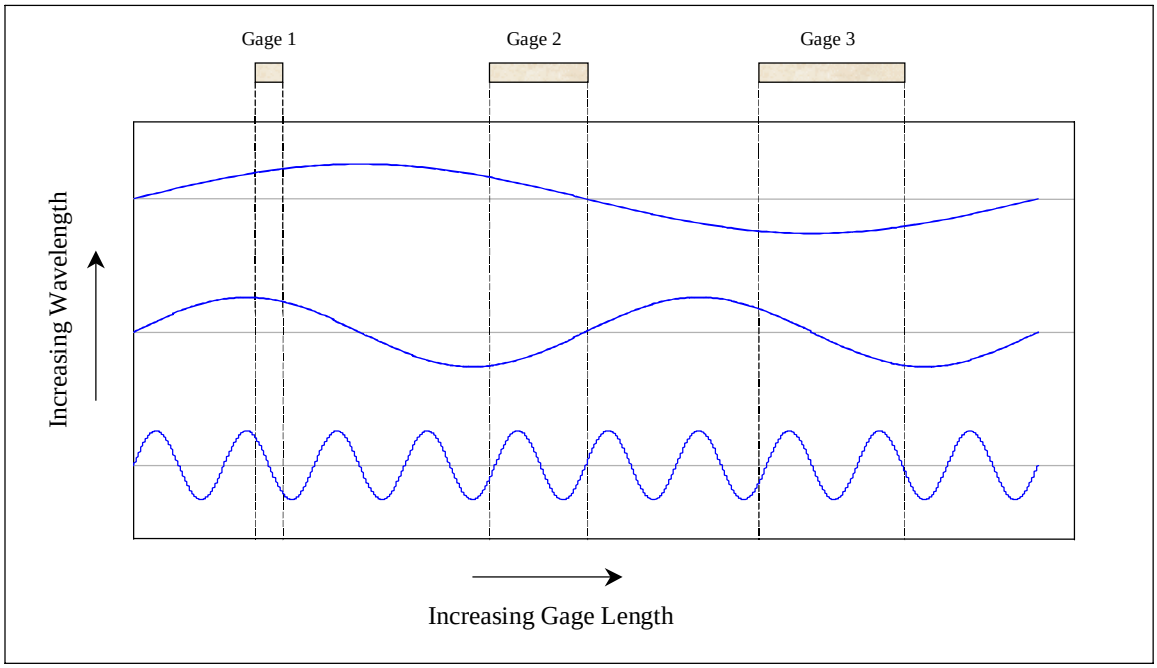

Figure 4.7 Plot of wavelength versus gage length

Imagine what the output of each gage would be (the average strain over the gage length). A number of interesting questions arise for these situations. The smaller the strain gradient across the element length, the closer the output will be to the true strain. Look at the special case where the wavelength is equal to the gage length (gage 2 – bottom strain curve). The average output is zero, but the actual strain is not! This will occur for integer multiples of the wavelength. As the wavelength decreases, so too does the ability to resolve the peak strain due to the averaging effect over the gage length. The peak strain is consequentially always estimated low. The following

diagram illustrates this point. Notice that the steeper the gradient (i.e. short wavelength), the less the peak strain can be resolved.

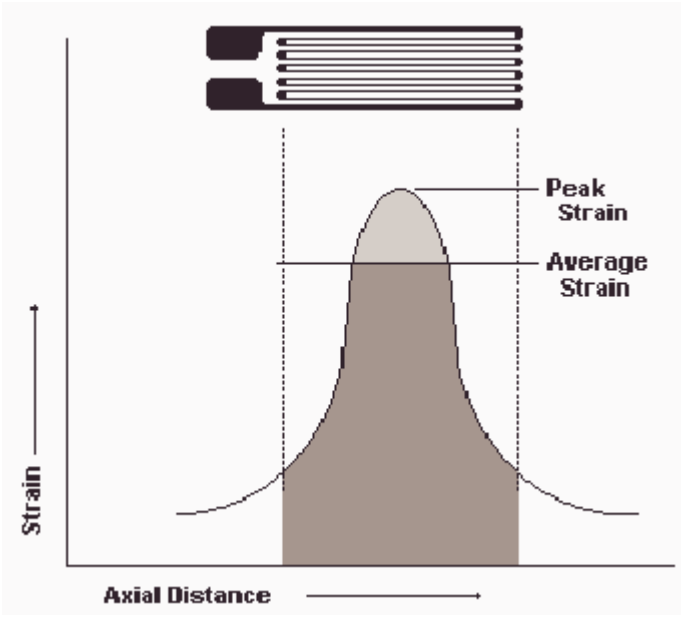

Figure 4.8 Averaging effect on peak strain *(from Measurements Group Inc.)*

For harmonic waves propagating through a strain gage, the peak output from the gage will always occur when the peak strain is centered in the gage, as illustrated in figure 4.8. To determine the closed form solution for the peak strain reported by a strain gage, the harmonic wave must be integrated over the gage length. By recognizing that the peak of a cosine wave coincides with the center of the gage, the following expression yields the peak strain reported by the strain gage. Remember the peak output of the gage is always less than the true peak strain.

$$\varepsilon_{\text{Re ported}} = \frac{C_o}{L} \int_{-\frac{L}{2C_o}}^{\frac{L}{2C_o}} \cos(2\pi \cdot f \cdot t) dt \qquad \textbf{(4.1)}$$

C_o, L, and f are the wave velocity, gage length, and frequency of interest, respectively. The evaluation of this integral yields an expression for the peak strain reported by a strain gage, given by equation 4.2.

$$\varepsilon_{\text{Re ported}} = \frac{C_o \sin\left(\frac{\pi \cdot L \cdot f}{C_o}\right)}{\pi \cdot L \cdot f} \qquad \textbf{(4.2)}$$

Upon examination of equation 4.2, one can see that the reported strain follows a sinc function. A plot of the reported peak strain versus frequency for a harmonic input of amplitude one is shown in figure 4.9. Notice that the shorter gages are more accurate at measuring high frequency strains.

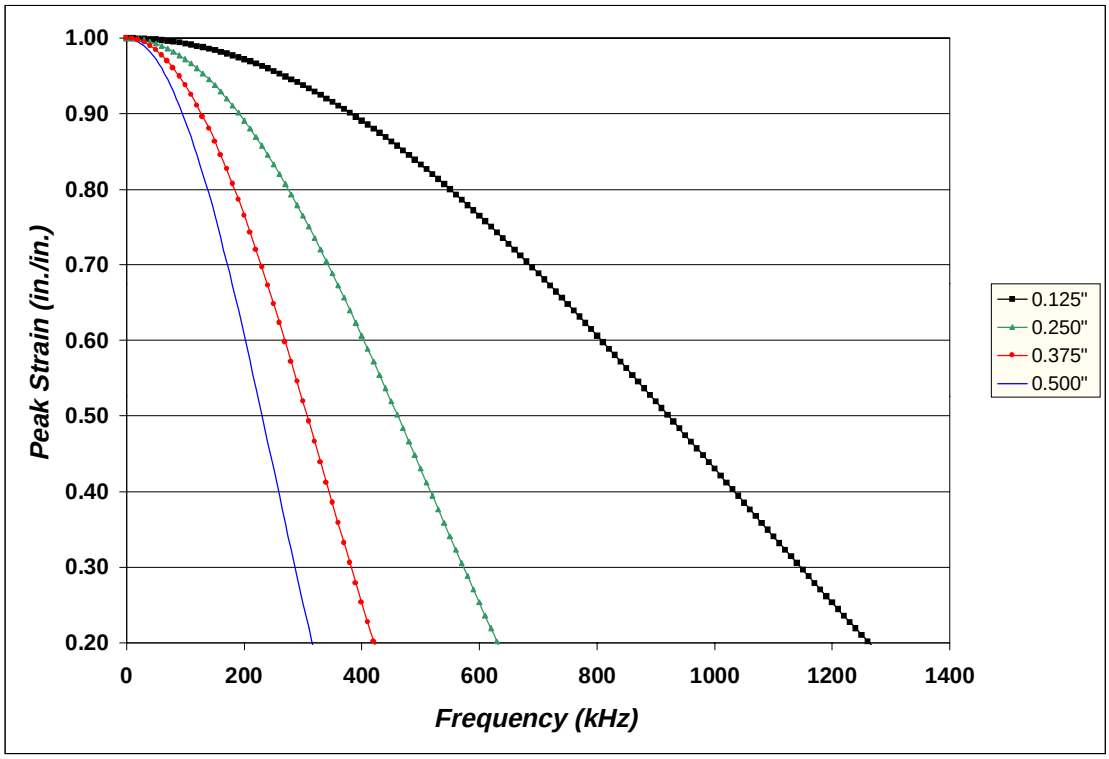

Figure 4.9 Reported peak strain from various gage length strain gages

Notice that for DC, accurate strain values are reported. As frequency increases, however, the actual strain becomes drastically attenuated. As was expected, shorter gages offer greater frequency response. The effect of the averaging dominates the output of the strain gage for high frequency. The output from the gage is zero when

the wavelength is equal to the gage length. To choose a strain gage, the desired accuracy of peak strain and frequency extension must be considered. According to the measurements Group, 'Strain gages of less than about 0.125 in (3 mm) gage length tend to exhibit degraded performance - particularly in terms of the maximum allowable elongation, the stability under static strain, and endurance when subjected to alternating cyclic strain.' Solving equation 4.2 with this gage length and properties of a steel bar, one attains the highest resolved frequency. For this case, cyclic strain frequencies must be less than 150 kHz to be a reasonably accurate representation.

4.4.2 CONVOLUTION OF MEASURED STRAIN

In the previous section, it was shown that the accuracy of strain gage measurements becomes limited for wavelengths on the order of the gage length. Another condition, related to the physics of the strain gage, exists that distorts the output. There is a windowing effect on all strain gage measurements that distorts the actual strain pulse. That is, the effective gage length represents a rectangular window that in effect changes the shape of the true strain pulse. To calculate the effect of windowing requires a convolution solution. Recall that convolution in time is equal to multiplication in frequency. That is, the inverse Fourier transform of the product of two functions of frequency is equal to the convolution of the two same functions in the time domain. Consider a square pulse of magnitude B and duration $P_L / 2$, measured by a rectangular window of magnitude A and length $G_L / 2$, both pulses having period T. The Fourier series of these pulses is shown in equations 4.3 and 4.4, respectively.

$$Pulse(\omega_o) = \frac{B \cdot P_L}{T} \cdot SINC\left(\frac{n \cdot \omega_o \cdot P_L}{2}\right) \quad \textbf{(4.3)}$$

$$Window(\omega_o) = \frac{A \cdot G_L}{T} \cdot SINC\left(\frac{n \cdot \omega_o \cdot G_L}{2}\right) \quad \textbf{(4.4)}$$

The frequency domain representation of the convolved output signal is given by equation 4.5.

$$\varepsilon_{OUT}(\omega_o) = Window(\omega_o) * Pulse(\omega_o) \qquad \textbf{(4.5)}$$

The convoluted time domain signal can thus be calculated from the inverse Fourier transformation of equation 4.5.

$$\varepsilon_{OUT}(t) = \sum_{-\infty}^{\infty} \frac{4 \cdot A \cdot B \cdot SIN\left(\frac{G_L \cdot n \cdot \omega_o}{2}\right) \cdot SIN\left(\frac{P_L \cdot n \cdot \omega_o}{2}\right)}{T^2 \cdot n^2 \cdot \omega_o^2} \exp(-i \cdot n \cdot \omega_o \cdot t) \qquad \textbf{(4.6)}$$

By plotting equation 4.6, the windowing effects of the strain gage can be seen. Though extremely complicated in form, equation 4.6 affords the investigator a means of predicting gage output for many configurations of gage lengths (G_L) and pulse lengths (P_L). Figure 4.10 is a plot of the convolved output of various pulse length – to - gage length ratios.

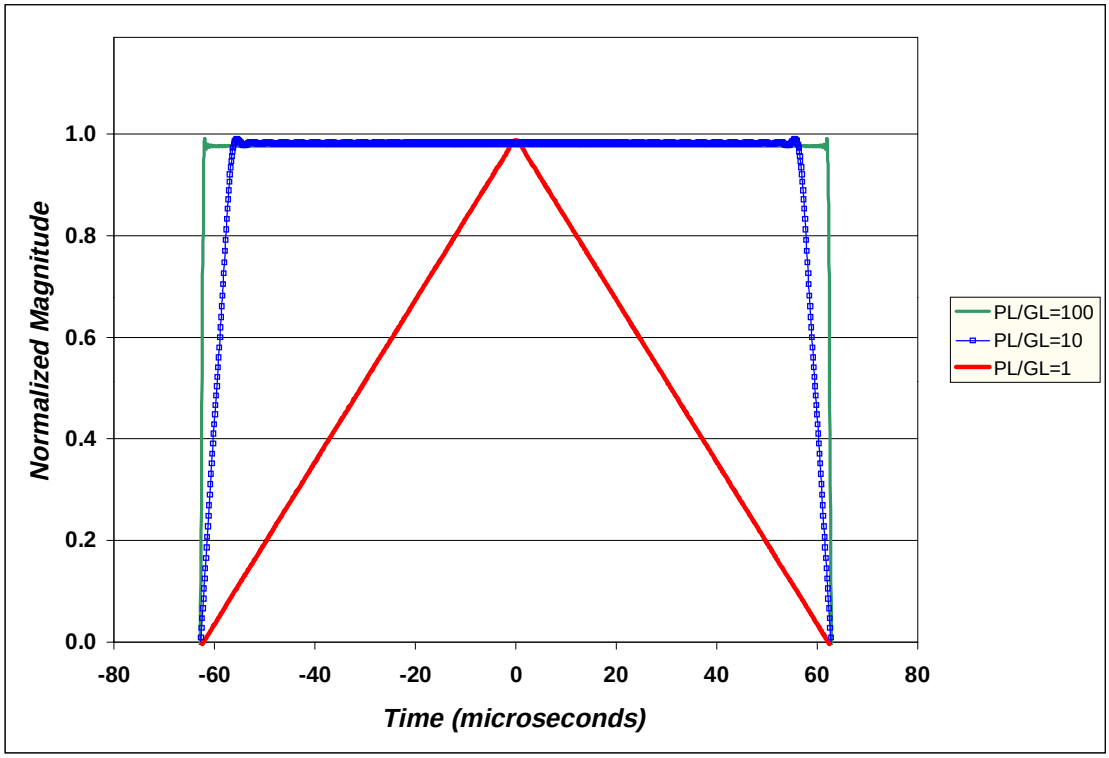

Figure 4.10 Convolved output of strain gages

Notice that all of the convolved pulses exhibit increased rise time, not characteristic of the square input pulse. This rise time is due to the period of time when the pulse just begins and just exits the strain gage. Just before entering the gage, the strain gage output is zero. As the pulse progresses through the gage, more and more of the gage length is deformed, until the point when all of the gage length is being deformed. In the limiting case where the gage length equals the pulse length, the maximum value is only reached at one time because there exists only one time when the gage window and pulse window perfectly overlap.

With the measured strain signals in hand, corrections for the windowing effect of the gage can be employed by dividing the Fourier transform of the strain signal by the Fourier transform of the gage measurement window.

4.4.3 SIGNAL CONDITIONERS

Many configurations exist for strain gages – some compensate for bending and temperature variations, others for torsion. The one-dimensional assumption for the pressure wave propagation implies that no bending or torsional effects exist. Though pressure bar bending is not a concern in split Hopkinson bar testing, any possible pressure bar bending can be compensated for in the strain bridge arrangement. By mounting two diametrically opposing strain gages, one can wiring the strain bridge circuit to remove any bending effects.

The digital oscilloscope used at the NSWCDD has no differential input. Therefore, a differential amplifier is required between the strain bridges and oscilloscope. Also, the low voltage signals from the strain gages must be amplified to match the dynamic range of the oscilloscope. To design an amplifier using simple op-amp technology requires that the desired gain and bandwidth be identified. An intrinsic and nearly

constant valued characteristic of operational amplifiers is called gain bandwidth. As its name suggests, gain bandwidth is the product of gain and desired bandwidth. As you raise the gain, the effective bandwidth is lowered, since this product remains constant for most op-amps. Early on in this research, some literature indicated that a frequency range up to 5 MHz was necessary for some Hopkinson bar tests. Had the nature of the strain transducers been fully explored at that time, efforts would not have been spent on designing amplifiers for this unnecessary frequency range. But efforts were spent and a lesson was learned, and fortunately using amplifiers with too high a frequency range is certainly better than too small. The design specifications of the amplifier circuits are a 5 MHz frequency range and a gain of twenty. All of the circuit design was done in MicroSim PSpice version 6.3a. The op-amps are Burr Brown OPA620, with supply voltages of 5 volts. Figures 4.11 and 4.12 are the amplifier characteristics in the frequency domain.

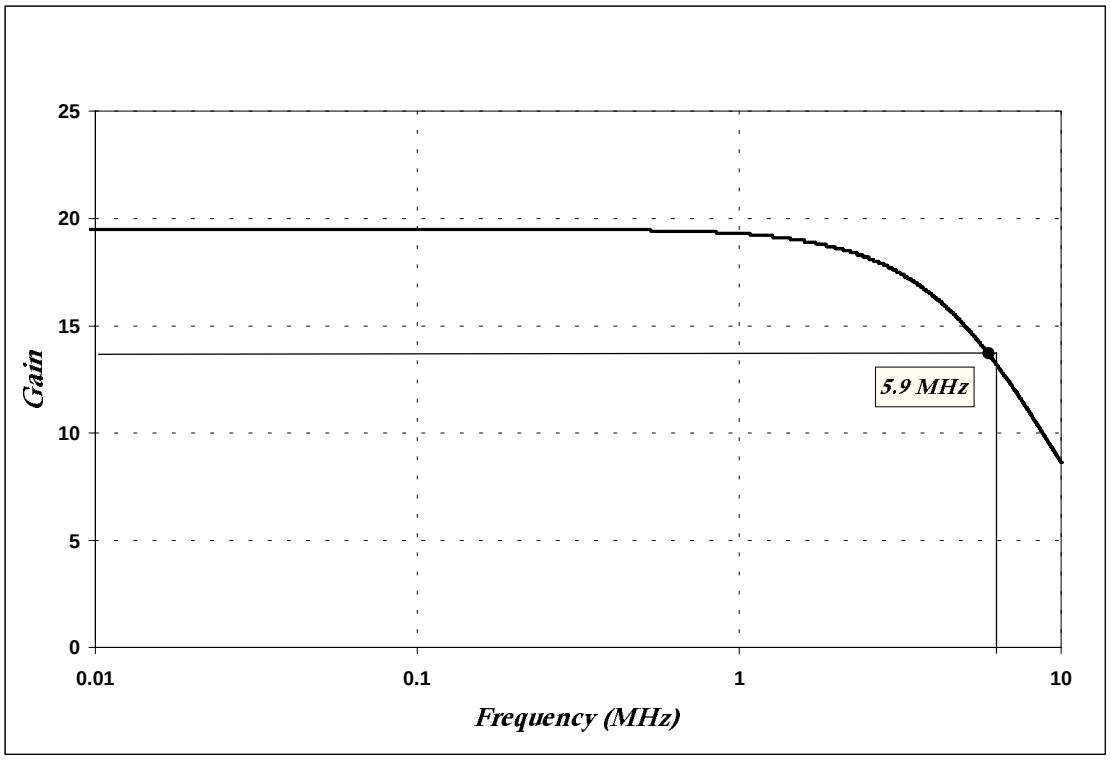

Figure 4.11 Amplifier Frequency Response Function

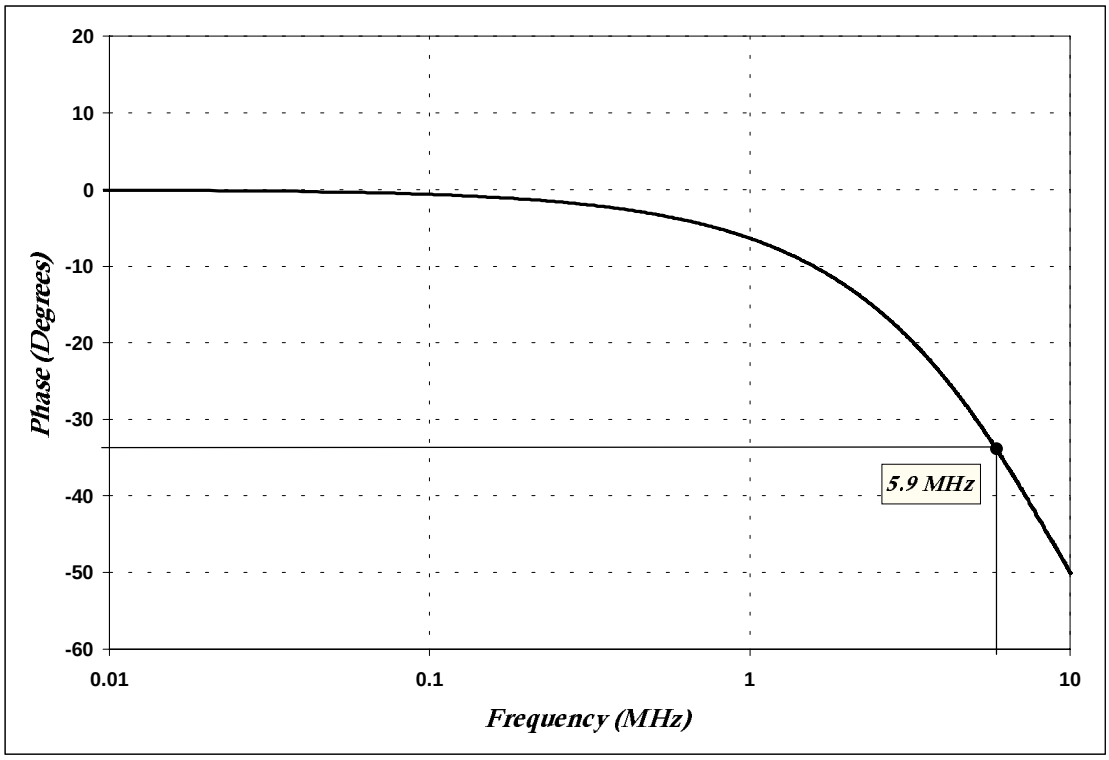

Figure 4.12 Amplifier Phase Response

Once amplified, a digital oscilloscope records the strain signals. The procedure taken for performing tests is outlined in the following section

4.5 TESTING PROCEDURE

To perform a SHPB test, certain decisions and preparations need be made. Firstly, the investigator needs to decide which specimen properties are of interest. Specifically, the desired strain rate and total strain must be determined prior to any testing. After deciding on the desired specimen properties, specific steps are taken to ensure that those properties are attained in the test. Figure 4.13 depicts a typical procedure followed for performing every test.

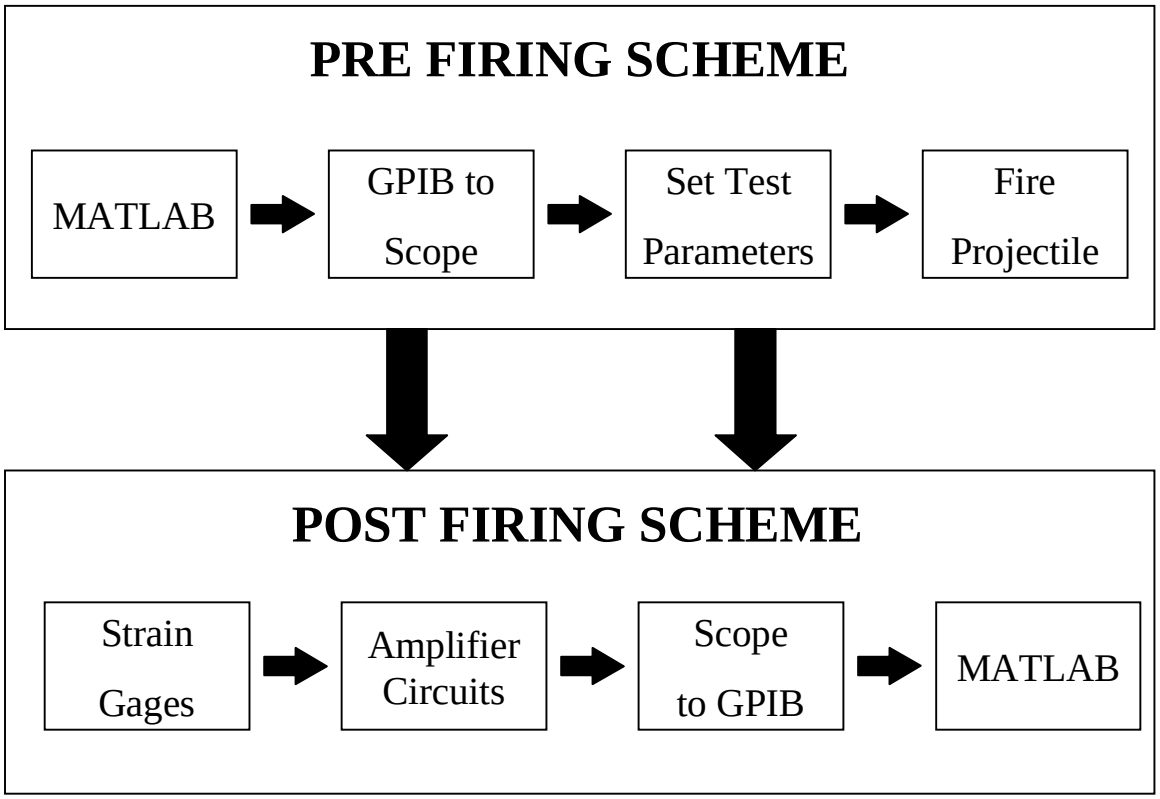

Figure 4.13 Block diagram of SHPB testing procedure

In the first block, the user inputs various parameters into a MATLAB interface, from which test specifications are calculated. The testing parameters required for most of the tests at NSWCDD are shown in figure 4.14.

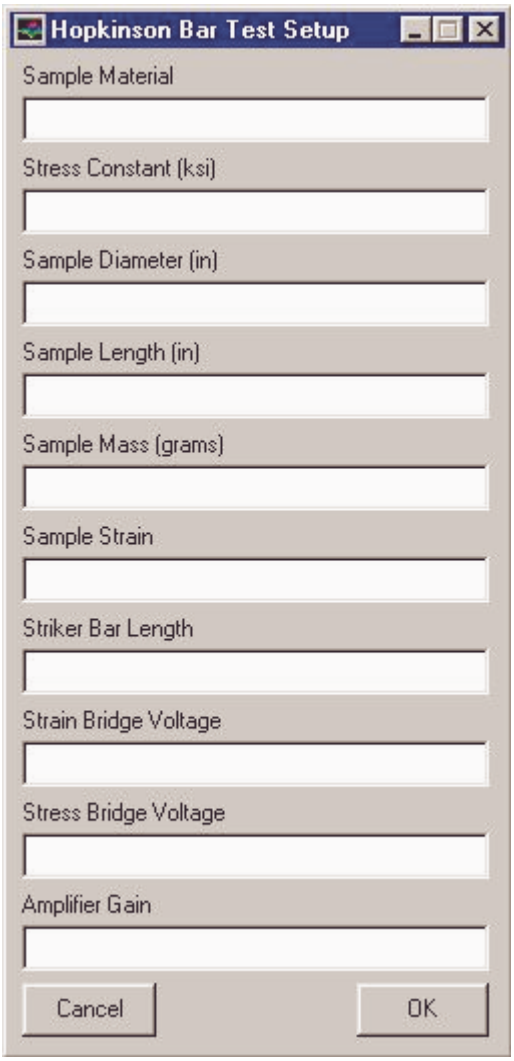

Figure 4.14 Input parameters for SHPB test

Based on the user input for these sample properties and desired total strain, the MATLAB routine calculates testing parameters, necessary to achieve that total strain. Based on these calculations, the investigator can setup the apparatus to the required specifications. Some of the more relevant testing parameters calculated in MATLAB are summarized in the following table.

Table 4.3 Test parameters calculated by MATLAB interface

Parameter	Function
Breech Pressure	Estimates the breech pressure required to achieve the necessary striker bar velocity
Incident Bar Stress	Makes sure that the stresses in the incident bar remain well below the yield strength of the bar material.
Sample Strain Rate	Estimates the strain rate the investigator should observe
Strain Bridge Output	Allows user to set the dynamic range of oscilloscope

Table 4.3 is by no means the complete list of calculations, but are the most crucial to setting up the apparatus and data acquisition. Once these parameters are calculated, one must physically adjust the SHPB apparatus for each test. Though not yet implemented, all of the necessary oscilloscope parameters will be sent directly from the PC to the oscilloscope, via GPIB. It is anticipated that the GPIB interface will greatly reduce setup time and accuracy from test to test, since the scope will be optimized for each test.

The operator must ensure that the entire apparatus is setup properly to conduct successful experiments. The setup includes lightly greasing the pressure bar – specimen interfaces, setting the gas gun pressure and packing the striker, and placing all of the protective shielding around the specimen.

Upon releasing the pressure from the gas gun, the striker bar is propelled into the incident bar. The compressive wave generated travels down the first bar, partially through the specimen, and continues propagating in the second bar. Strain gages mounted in the middle of each pressure bar respond to the instantaneous strains generated from the impact event. These strain signals are then amplified and digitally captured. The captured signals are then sent back to the PC via GPIB for the necessary data analysis. All of the data analysis has been performed on an IBM PC in the MATLAB programming environment.

4.6 DATA PROCESSING PROCEDURE

Once the data are shipped back into the PC, several manipulations must be done prior to generating the dynamic stress-strain relations of the specimen. All of the data processing is done in MATLAB. Figure 4.15 shows a typical progression through the data processing procedure.

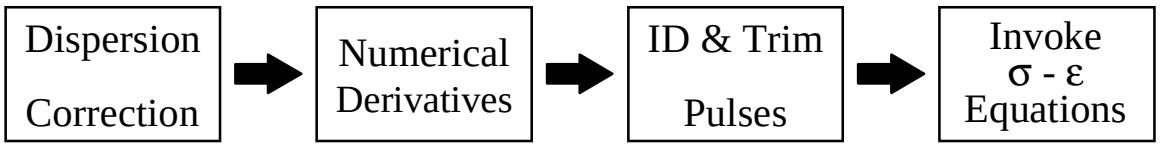

Figure 4.15 Block diagram of typical data processing procedure

The signals must first be corrected for the dispersion. Typical incident and transmitter bar strain signals are shown just below. Notice the trapezoidal shaped incident pulse and the oscillatory nature of the reflected pulse.

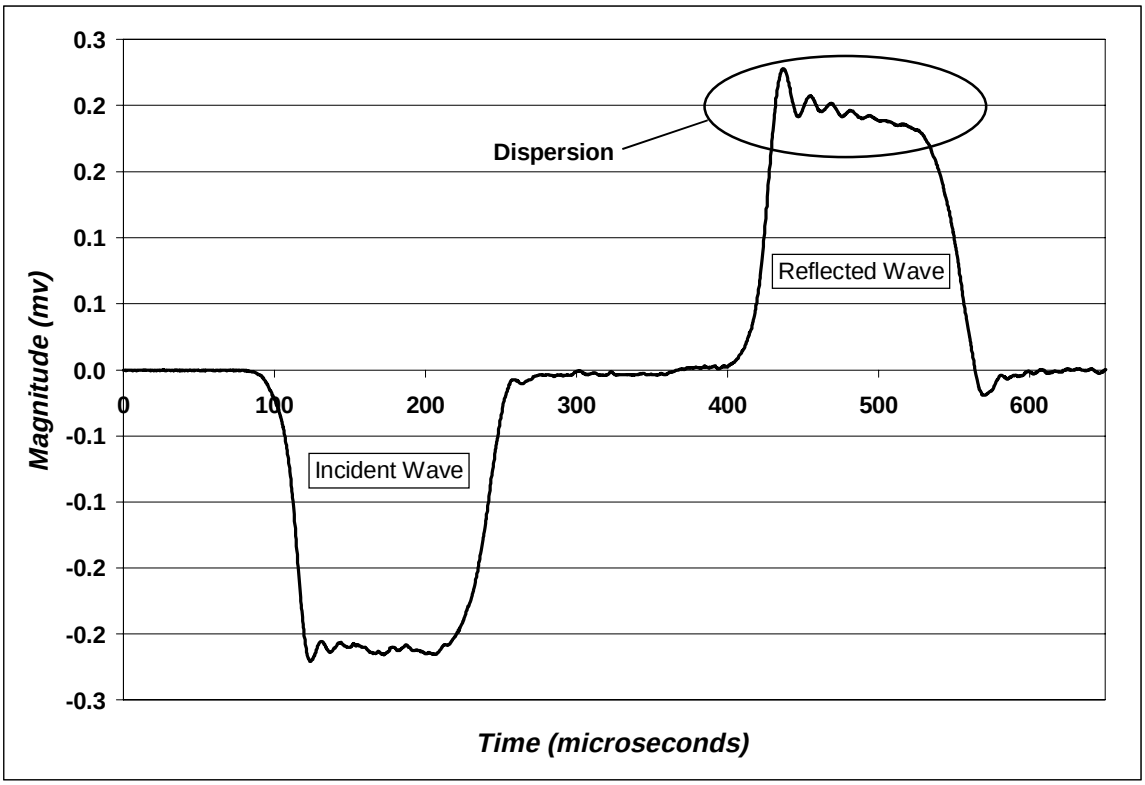

Figure 4.16 Typical incident strain history

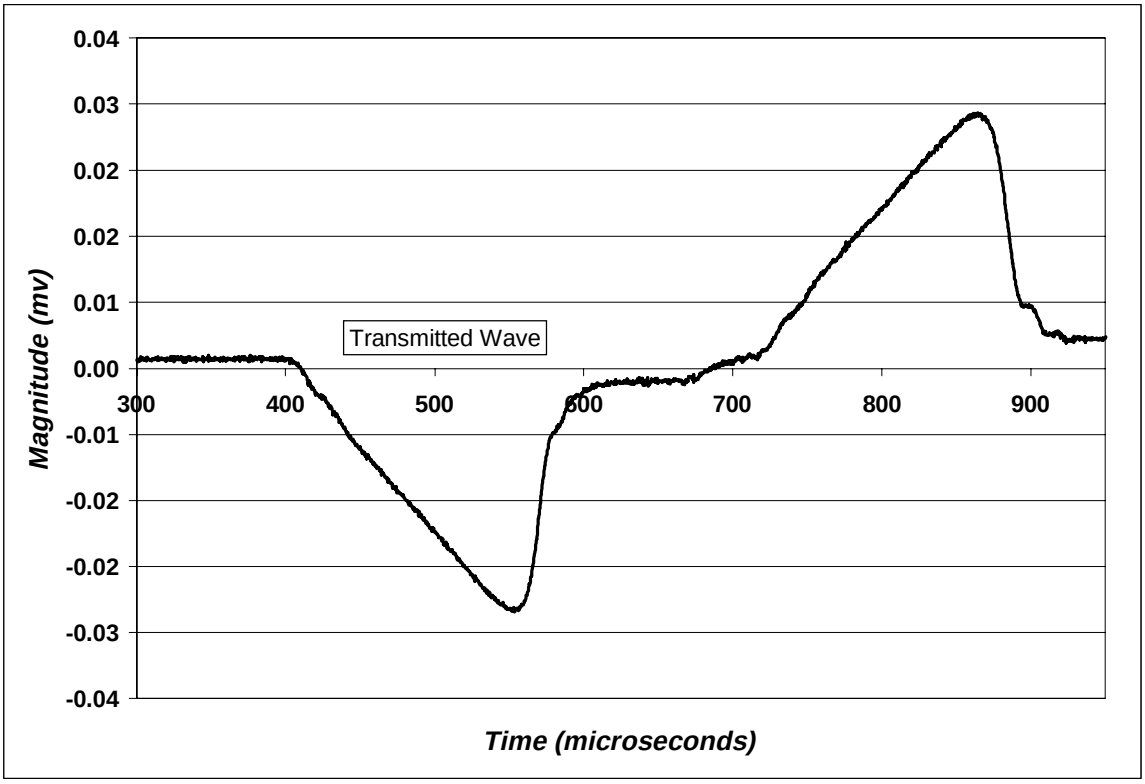

Figure 4.17 Typical transmitted strain history

4.6.1 DISPERSION CORRECTION

As was discussed in chapter three, dispersion in the pressure bars masks the actual shape of the pulse. To nullify the effects of dispersion in the frequency domain requires that an appropriate phase shift be employed to each spectral component. By calculating the complex Fourier transform of each strain pulse, the phase was adjusted according to equations 3.38 and 3.39, shown here for convenience.

$$F_{corrected}(t) = \frac{1}{N}\sum_{n=1}^{N}\left[A_n \cos(2\pi f \cdot nt + \phi) + B_n \sin(2\pi f \cdot nt + \phi)\right] \qquad \textbf{(3.38)}$$

$$\phi = 2\pi f \cdot n\left(\frac{1}{C_o} - \frac{1}{C_n}\right)y \qquad \textbf{(3.39)}$$

The theoretical velocities calculated by Bancroft were used to calculate the phase, ϕ. The experiments necessary to ascertain the actual bar velocities (Section 3.7) were not performed in time to be included in this thesis. Once these experiments are conducted, it is anticipated that their use will be implemented shortly there after.

4.6.2 STRESS AND STRAIN PULSE IDENTIFICATION

The unknown transit time through the greased joint and sample hinders the precise identification of the pulse start and end difficult. Normally one would expect a short transit time, which is the case, but since the impact events have such short duration (often only 100-200 μs) small time unknowns yield large errors when aligning the two pulses together. The start of each pulse must be identified properly to enable an accurate construction of the dynamic stress-strain curve. Previous investigators have attempted to identify the pulses based on the estimated time required for the pulses to travel along the bars, through the specimen and to the strain gages. Unfortunately this requires that the wave velocity be known for all samples prior to testing. Further, since the pressure bar – sample interfaces need lubrication, the effects of the grease on transit time introduces another unknown. In lieu of this time-based pulse identification, a means of identifying the pulses incorporating a high accuracy numerical derivative algorithm to each of the strain histories is used. By means of identifying changes in slope, the appropriate pulses may be identified without any specific reference to time, no prior knowledge of sample wave velocities, and no dependence on the unknown grease effects.

To consistently identify pulses, in a systematic way, requires numerical procedures. By estimating the derivatives of the strain pulses, a code can search for changes in slope. For a perfect strain history, both the strain and strain derivative leading up to the pulse edge would be zero. The measured strain, though close to zero is never identically zero due to noise. Since noise is by nature random, so too are its derivatives. Therefore to identify the edges of the pulse, a code must search for a number of consecutive derivatives containing the same sign. For example, to identify

the start of the compressive incident pulse, the code searches through the derivatives 'looking' for say ten consecutive negative derivatives. Since it is highly improbable for ten consecutive same sign derivatives of noise to exist, the code always finds the edge of the pulse. In fact, the probability of 10 consecutive random derivatives is one in 2^{10}, or about 0.1 percent. The highest observed number of consecutive, same sign derivatives of noise is five, which would lead to a maximum error in the pulse start of 5 divided by the sampling rate.

The numerical derivative algorithm employed is a high accuracy forward finite-divided-difference formula [18] given by

$$f'(x_i) = \frac{-f(x_{i+2}) + 4f(x_{i+1}) - 3f(x_i)}{2h} \qquad \textbf{(4.7)}$$

where *i* is the index number referencing the data point number and *h* is the sample rate of the signal. Recall that the specimen stress, strain, and strain rate are all calculated from the pressure bar strain pulses. Specimen strain is simply the strain rate integrated. The equations necessary for these calculations were developed in chapter 3 and employed verbatim. An integration routine using a modified trapezoidal rule was implemented for calculating the specimen strain.

With a means to acquire and process data, the next step is to interpret and improve testing techniques. This is the focus of the next chapter.

CHAPTER 5

TEST EVALUATION AND INTERPRETATION

5.1 INTRODUCTION

This chapter presents suggestions towards improving testing conditions. A technique for minimizing the effects of dispersion is introduced. A discussion of optimizing the sample diameter based on the pressure bar - sample impedance mismatch is followed by a statistical interpretation of copper data. Comparisons of highly dynamic tests are compared to static tests.

5.2 TESTING BENEFITS FROM SHAPING THE IMPACT PULSE

The impact of two collinear rods results in a square wave with a length twice that of the striker bar. A number of characteristics make square waves attractive for use in Hopkinson bar testing. They instantaneously reach a maximum value, which would seem to result in a constant strain rate test of long duration. For numerous reasons, outlined in the remainder of this section, square waves are in fact the worst shape when analyzing Hopkinson bar data.

5.2.1 MINIMIZING EFFECTS FROM PRESSURE BAR DISPERSION

In chapter three it was shown that pressure bar dispersion is due to the wave velocities dependence on frequency. It was suggested that waves with a narrower frequency bandwidth suffer less from the distorting effects of dispersion. The fact that the Fourier series of a trapezoidal shaped pulse contains fewer significant terms than that of a square wave suggests that efforts should be made at 'shaping' the impact pulse, perhaps by extending the rise time. An important tradeoff for increasing the rise time is that the peak value has a shorter duration. Since most investigators are interested in material properties at a given strain rate, it is often desired to reach that rate as quickly as possible. Data collected before the maximum is in fact useless for materials highly sensitive to strain rate. Therefore investigators must find a rise time short enough to

allow adequate material characterization, but long enough to significantly reduce the dispersive effects.

The two most common techniques used to shape the impact pulse are placing a compliant material between the striker bar and input bar, and machining the end of the striker bar into a dome shape. Since the latter technique raises concerns over the one-dimensional wave requirement, impact plenums have been investigated for the purposes of wave shaping. This has been largely in part a process of successive approximation. For the current investigation, the effects of various diameter copper plenums of 0.016" thickness were examined. The results on rise time are best seen visually, as is depicted in figure 5.1.

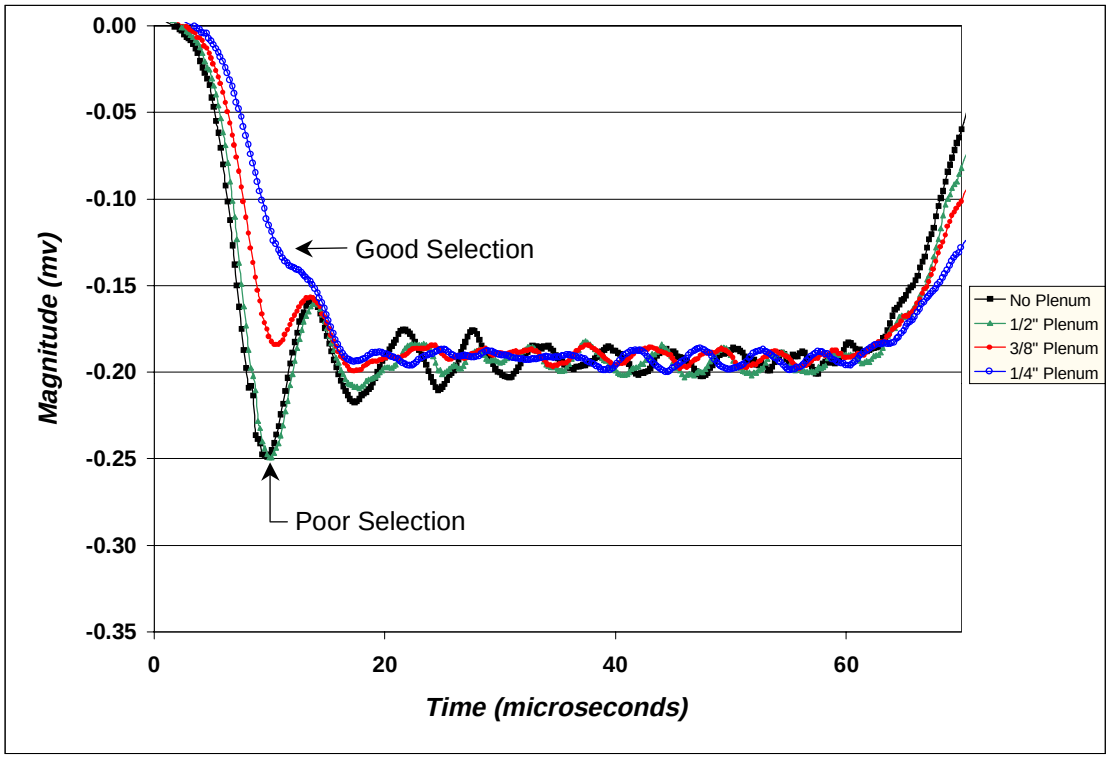

Figure 5.1 Plenum size impact on pulse shape

The large oscillations associated with pulse 'no plenum' and '½" plenum' render them poor candidates for selection. The pulse marked as 'good selection' is a desirable shape since the oscillations are small and the width of constant amplitude is large.

5.2.2 FURTHER APPLICATIONS OF WAVE SHAPING

Recall that the strain rate of a given material is calculated from the amplitude of the reflected pulse. In general, ductile materials harden during plastic deformation, termed strain hardening. This phenomenon manifests itself as an increase in the stress-strain curve. As a square wave deforms a specimen, the strain hardening of the specimen tends to decrease the rate of strain, evident by the negative slope of the reflected wave. To perform constant strain rate tests for ductile materials, the impact wave should be shaped to have a positive slope proportional to the amount of strain hardening in the specimen. For a positive sloped wave deforming the specimen, the strain hardening of the specimen decreases the strain rate to a constant value. Therefore impact wave shaping can in fact offer significant benefits, when evaluating materials.

5.3 INTERPRETATION OF IMPEDANCE EQUATIONS

In section 3.3.2, expressions were developed for the behavior of a wave as it encounters a step change in impedance. Transmission coefficients were defined as the ratio of the transmitted stress to the incident stress. Recall that the transmission coefficient is a number ranging in value from zero to one, zero representing total reflection and one representing 100% transmission. Typically the transmitted pulses are of substantially lower magnitude than the reflected pulses for materials tested in the Hopkinson bar. For some very low impedance materials, the transmitted stress wave is of such diminutive value, that the signal-to-noise ratio (S/N) becomes too small to process the signal. One way to improve Hopkinson bar test results would be to choose a diameter resulting in the reflected and transmitted pulses having similar magnitudes. This would result in comparable signal-to-noise ratios for the two

signals. By choosing an inappropriate diameter, the S/N ratios can differ by as much as a 25 dB. By applying the same theory as for other transmission coefficients, the transmission coefficient from bar 1 to bar 3 can be determined. Again solving for the sample diameter yields equation 5.1.

$$D_S = \frac{D_{BAR} \cdot \sqrt{(\rho c)_{BAR}} \cdot \sqrt{\left(2 \cdot \sqrt{(1-\alpha_{13})} + \alpha_{13} - 2\right)}}{\sqrt{\alpha_{13}} \sqrt{-(\rho c)_S}} \qquad \textbf{(5.1)}$$

Though rather complicated in equation form, plots of diameter versus transmission coefficient for various materials supports practicality, shown in figure 5.2.

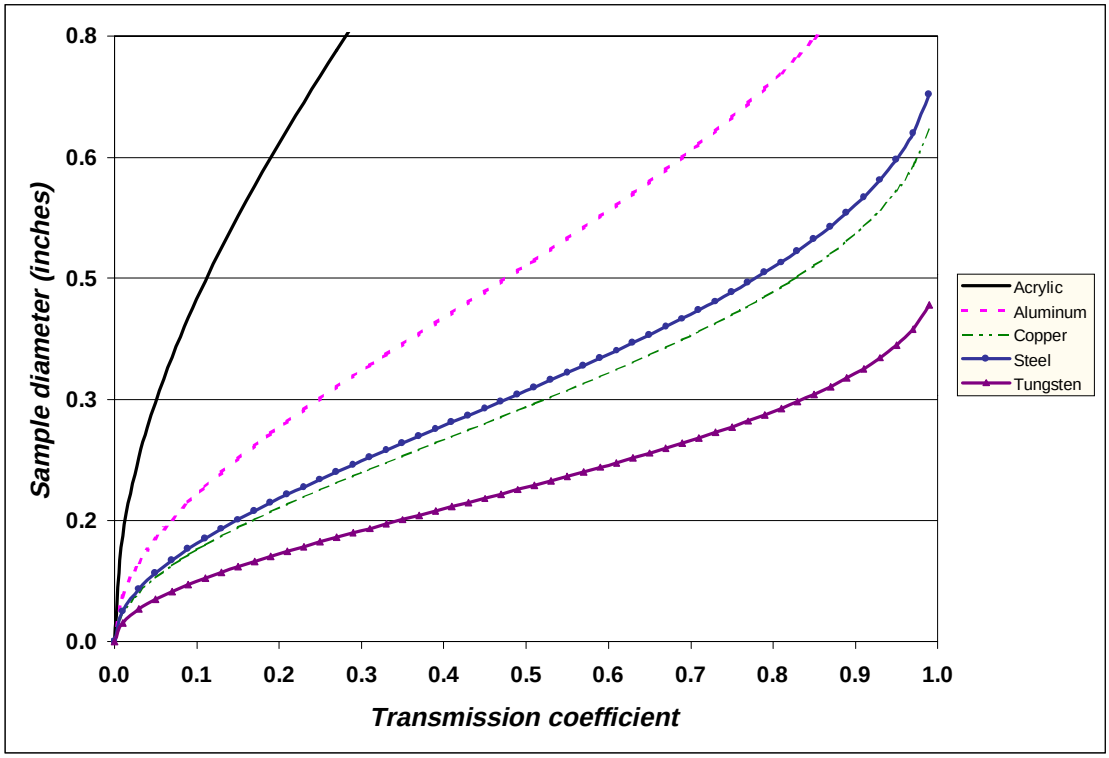

Figure 5.2 Sample diameter vs. α_{13} for common materials

Notice that as the sample diameter decreases, the magnitude of the reflected pulse increases ($\alpha \rightarrow 0$). A transmission coefficient of 0.5 physically means that the reflected

and transmitted pulses have equal magnitudes. For some low impedance materials it is not possible to achieve large transmission coefficients. The results of testing these materials (Plexiglas, lexan, and other acrylics) should be suspect of error. The following table lists some impedances for common materials.

Table 5.1 Acoustic impedances for common materials (modified from CRC's Handbook of Tables for Applied Engineering Science)

Material	***Density (ρ) (lb/in^3)***	***Plane Velocity (in/s)***	***Acoustic Impedance (ρc) ($lb/in^2 \cdot s$)***
Acrylic	*0.0428*	*106,304*	*4,545*
Aluminum	*0.0975*	*251,981*	*24,561*
Steel	*0.2780*	*198,818*	*55,265*
Copper	*0.3345*	*188,985*	*63,216*
Tungsten	*0.7078*	*206,703*	*146,304*

Consider the transmitted stress pulse through a specimen of lexan, shown in figure 5.3.

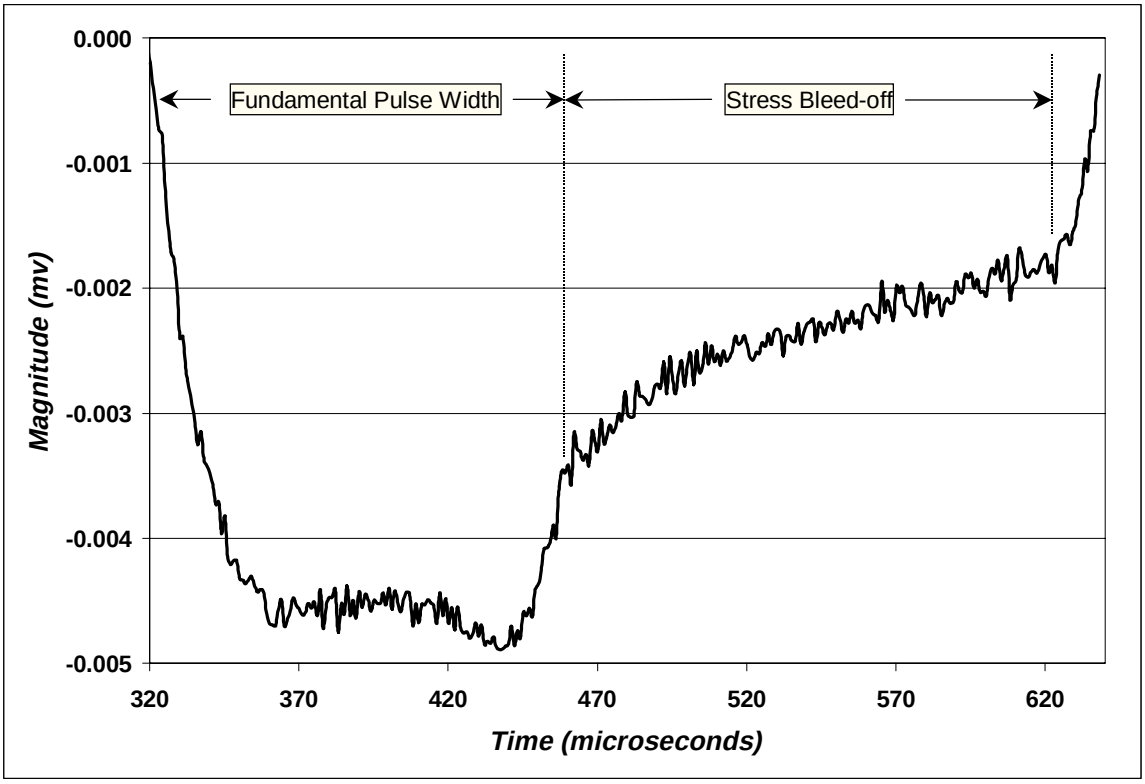

Figure 5.3 Transmitted stress pulse through sample of lexan

Two regions have been identified – fundamental pulse width and stress bleed-off. The first region of the plot has a total duration equal to that of the impact. The second region is due to the stress wave being 'trapped' in the specimen. Hence, the stress pulse gradually exits the sample. For materials whose impedance is much lower than that of the pressure bars, the waves have trouble exiting the sample. To determine how much bleed-off should be expected recall the expression for the fraction of a wave leaving the specimen.

$$\alpha_{23} = \frac{2s_2(\rho c)_3}{s_2(\rho c)_2 + s_3(\rho c)_3} \qquad \textbf{(3.12.2)}$$

For cylindrical bars and samples, one can solve for the sample diameter, given by equation 5.2.

$$D_S = \frac{D_{BAR}\sqrt{\alpha_{23}}\sqrt{-(\rho c)_3}}{\sqrt{(\alpha_{23}(\rho c)_2 - 2(\rho c)_3)}} \qquad \textbf{(5.2)}$$

where D_S, D_{BAR}, α_{23}, ρc_2, and ρc_3 are the sample diameter, pressure bar diameter, transmission coefficient from sample to transmitter bar, and the sample and pressure bar impedance, respectively. By plotting equation 5.2 it becomes very obvious that small diameters yield low transmission, thus the wave stays trapped in the specimen longer.

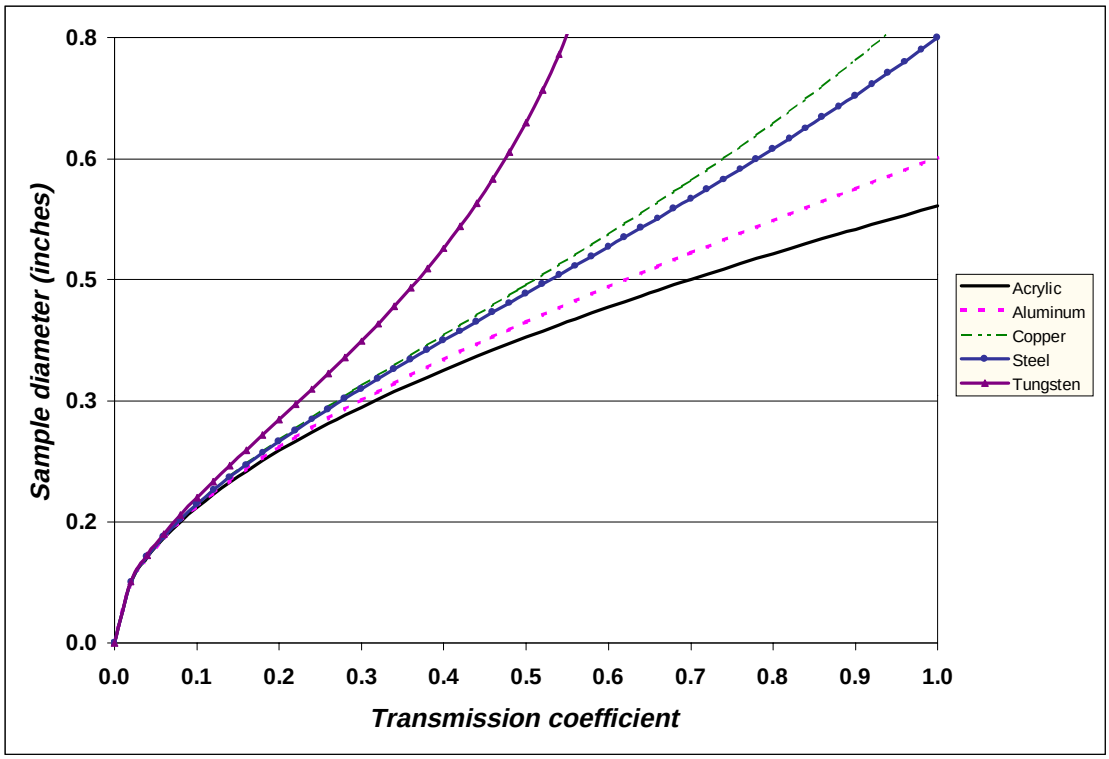

Figure 5.4 Sample diameter vs. α_{23} for common materials

Figure 5.4 shows that the transmission coefficient is only 10% for a sample of 0.2" diameter lexan. This means that the wave is reflected back and forth in the sample, losing only 10% of its peak value per reflection. The phenomenon of bleed-off always exists, but has a much greater effect when the diameter is small. By carefully

selecting a sample diameter, the quality of the input and output signal will be nearly equal.

5.4 STATISTICAL CONSIDERATIONS

When measuring various quantities, one should always be concerned with how repeatable the data are. Each additional measurement of the sample stress and strain increases the investigator's faith, per se, in their reliability. The variance of any one test is infinite; therefore many tests must be performed to become confident in results.

For every stress value from a stress-strain curve, a corresponding value of strain exists. The magnitude of the stress and strain are determined from the pressure bar strains, as developed in chapter three. An interesting problem arises when attempting to compare the results of one test to another. When plotting the stress-strain data pairs for many sets of tests, one can qualitatively determine if they all have the same general trend by visual inspection. To compare multiple tests quantitatively poses a challenge due to various factors including sampling rate, noise, differentiation, etc. To illustrate the most significant challenge, consider the line given by $y = ax + b$, sampled at different locations (figure 5.5).

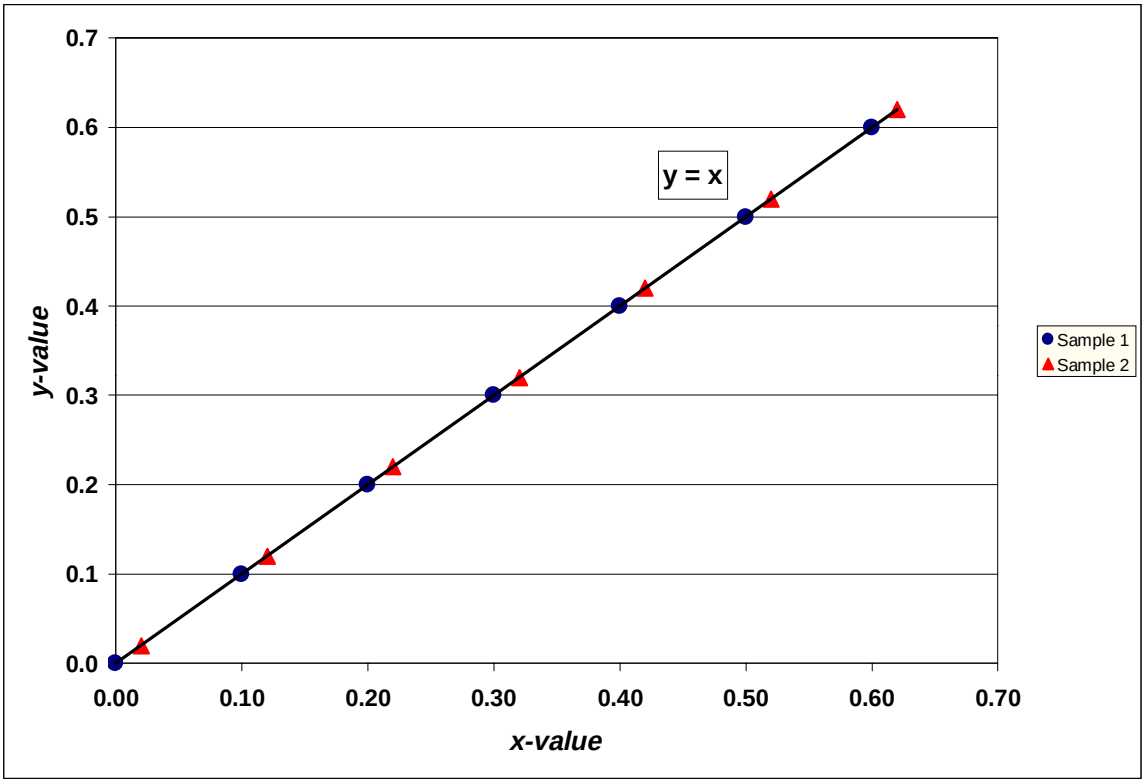

Figure 5.5 Plot of $y = ax$ for two given sampling locales

Obviously all of the data points lie along the same line with fourteen unique data pairs, seven from Samples 1 and 2. To compare the two sets of data one can either compare the coefficients from curves, fit to each data set, or interpolate for common values of y or x between the two data sets. For the graph above, it seems relatively obvious that one should compare the two data sets by examining the coefficients of a linear fit to each set. This comparison works only because the linear nature of the curve, known in advance. For stress-strain curves, it would be desirable to pass a curve through all of the data points, minimizing the deviation from all data points. This would require an extensive study of each material for the coefficients of the curve to have any real meaning; therefore the stress-strain data has been interpolated to find common values of stress and strain among all of the data sets. One important fact to recognize about interpolation is that the true error will always be greater than the interpolated error. If an infinite set of stress-strain pairs were available, there would be no error introduced.

The author has fit the data sets with a cubic spline to interpolate for common values of stress and strain. By using data generated from cubic splines, the true statistical values can not be attained. However, since the number of data pairs is so abundant, the errors introduced by cubic interpolation is minimized. To fully explore the statistical significance of Hopkinson bar data sets requires an in depth analysis of the nature of the stress-strain relations in the plastic region. Once a model is generated for the stress-strain behavior of a material, appropriate curves can be fit to each data set, from which these curves can be compared statistically. For the work presented in the following section, cubic splines were used to fit the data sets, since no models were available. Again since the number of data points is so great, errors are expected to be small from using the splines.

5.4.1 STATISTICAL EVALUATION OF COPPER

Several tests have been performed on copper, to generate stress strain curves at a strain rate of 2750 s^{-1}. By fitting ten data sets with cubic splines, common values for stress-strain data pairs were found, from which the arithmetic mean and standard deviation was calculated, plotted in figure 5.6 and 5.7.

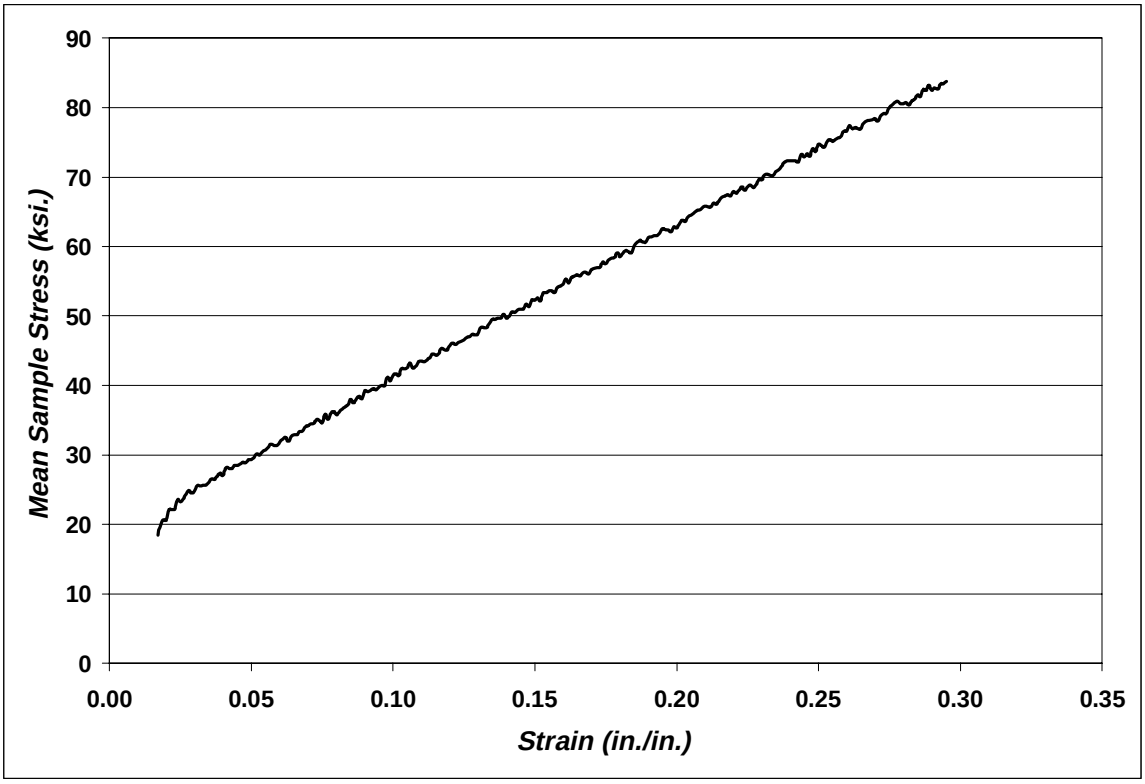

Figure 5.6 Mean value of engineering stress-strain of copper at 2700 s^{-1}

The initial portion of the stress-strain curve has been omitted since this portion represents where the impact pulse magnitude is rising and has therefore not reached a peak strain rate. The monotonically increasing nature of the curve is indicative of strain hardening.

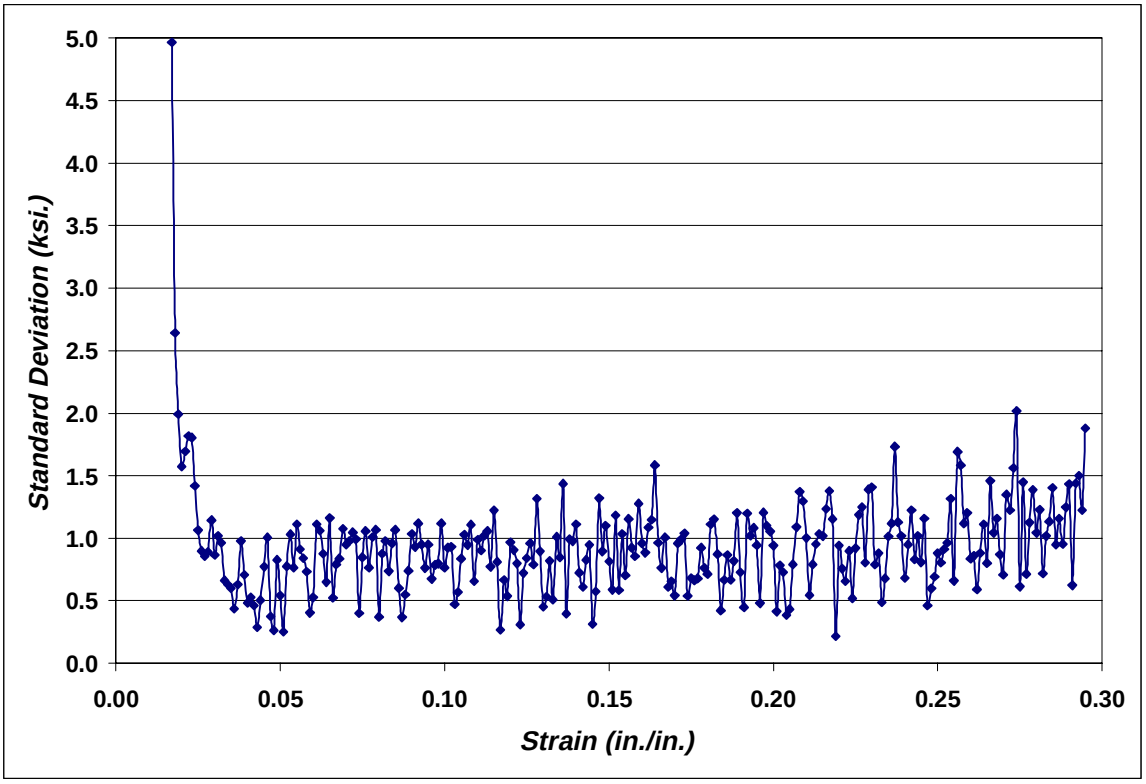

Figure 5.7 Standard deviation of all copper data sets

The standard deviation shows a widely scattered initial portion, followed by a random distribution beyond about 3 percent strain. Again, this is due to the changing strain rate early on in the test. The magnitude of the standard deviation remains largely between 500 and 1500 psi. By dividing the standard deviation by the stress, a plot of percent error can be generated, as shown in figure 5.8.

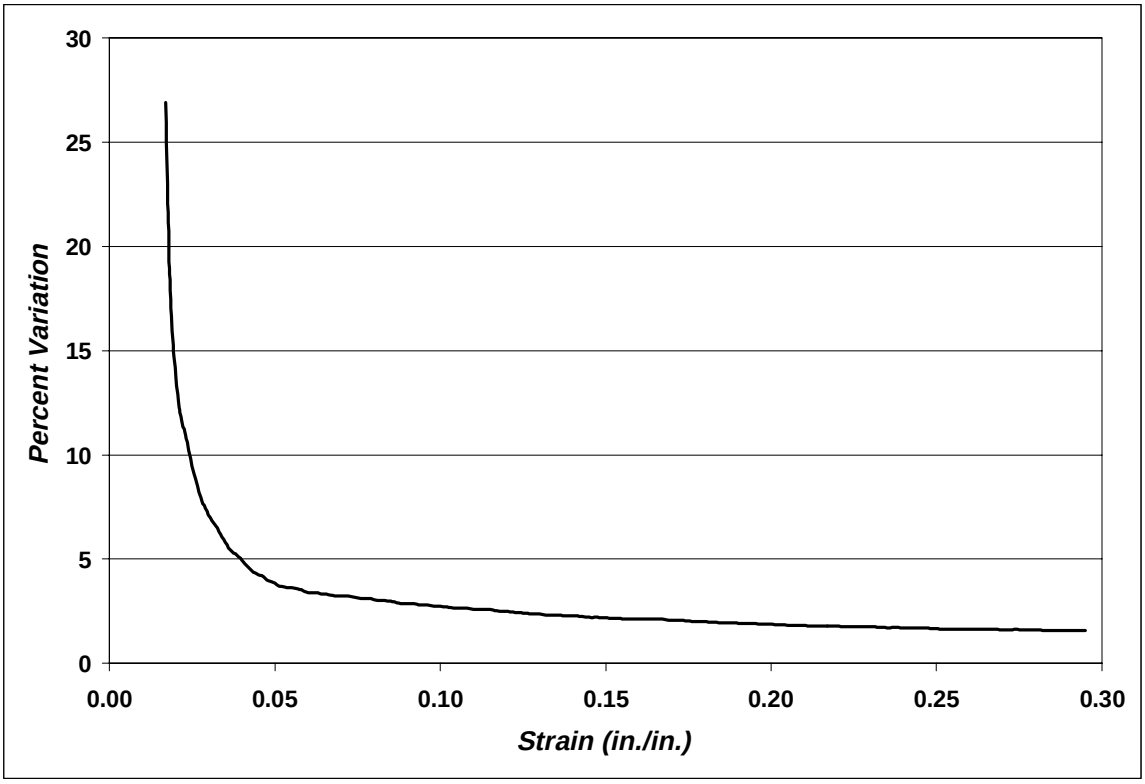

Figure 5.8 Percent variation from mean value

The percent variation continually decreases as the test progresses. A method that in effect improves testing accuracy is presented in the following section.

5.5 COMPARISON OF STATIC AND DYNAMIC STRESS-STRAIN CURVES

As the rate of deformation increases, so too does the strength of the material. In fact, Shigley stated that at extremely high strain rates, the yield strength approaches its ultimate strength. The copper evaluated in section 5.4 was deformed at a rate of 2750 in./in.-s. Similar samples were tested in a static compression test in Virginia Tech's Engineering Science and Mechanics Department. The resulting stress-strain curves for both the dynamic and static tests are shown in figure 5.9.

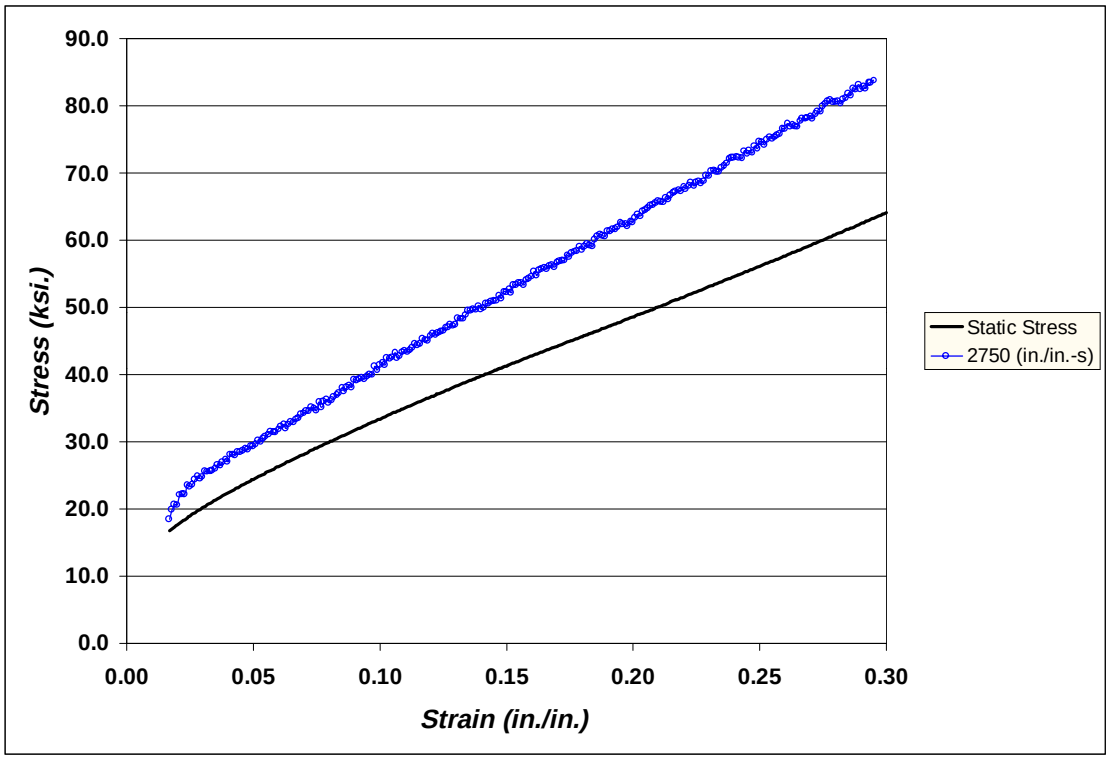

Figure 5.9 Static and dynamic stress-strain plot of copper

Two distinguishing characteristics are apparent when examining the static and dynamic curves. As was anticipated, the dynamic curve is of larger stress for the same degree of strain. The increased slope for the dynamic curve was rather unexpected and it is suspected that friction between the specimen and pressure bars has influenced the actual stresses for any given strain. That is, the interface friction restricted the expansion of the sample, therefore requiring a larger stress for a given strain.

For short, stubby samples, friction dominates the deformation, often resulting in a barrel shaped specimen. By lubricating the ends with a thin layer of grease, these frictional effects can be minimized. If a specimen's length-to-diameter ratio is too high, the sample will buckle during the test (rendering that test invalid). Dr. Norman Dowling, of Virginia Tech, has suggested choosing an L/D ratio of three for ductile materials [19]. For brittle materials an L/D in the range of 1.5-2 should be suitable.

CHAPTER 6

CONCLUSIONS & RECOMMENDATIONS

6.1 INTRODUCTION

The intent of this thesis was not to determine material properties for many different materials. Rather, improvements to the current techniques for ascertaining these properties and interpretations of various data were introduced. By carefully considering the requirements of transducers, data analysis techniques, and sample dimensions, improvements have been contributed toward Hopkinson bar testing.

6.2 SUMMARY AND CONCLUSIONS

Testing techniques have been evolving since the introduction of the split Hopkinson bar in 1913. It has only been the last decade or so, however, that significant data processing advancements have been possible. The author has made specific advancements in the following areas:

1) A technique to better align the stress and strain pulses using changes in slope instead of absolute time

2) An optimization technique, per se, for determining specimen diameter based on the impedance mismatch occurring at the interface of two materials

3) A technique for determining dispersive properties of longitudinal bars using existing Hopkinson bar apparatus.

Other techniques for producing favorable testing conditions were discussed in various sections of the thesis. Many more areas of research and development exist, which are expected to greatly enhance the use of the Hopkinson bar. Specific areas of interest to the author are outlined in the following section.

6.3 FUTURE AREAS OF RESEARCH AND ADVANCEMENT

Various conditions must exist for the specimen under investigation to deform homogeneously. Many investigators have been concerned with this particular aspect of Hopkinson bar testing and have made significant advancements. A comprehensive study of the dynamics influencing specimen deformation should lead to a more complete understanding of how to improve tests. Further an investigation of the pressure bar – specimen interface area mismatch is expected to lend valuable insight towards smarter testing.

Though many investigators have examined the effects of specimen length-to-diameter ratio, none have arrived at exactly the same conclusions. It would behoove NSWCDD to conduct tests to evaluate the influence of specimen geometry on predicted stress-strain behavior. These tests should be made in conjunction with the sample diameter selection based on impedance mismatch between the pressure bars and sample.

Further efforts should be made towards impact pulse shaping. By placing various materials between the striker bar and pressure bar, the rise time of the impact pulse can be extended, which in effect reduces the overall frequency bandwidth of the pulse. As the bandwidth is decreased, so too are the effects of dispersion. Many materials strain harden as they are plastically deformed. This hardening manifests itself as an inclined slope on the stress-strain curve. If one can select a plenum that shapes the impact pulse with a slight incline, the reflected pulse will be much flatter leading to a more constant strain rate test.

The use of strain gages for pulses of very short duration becomes limited in the Hopkinson bar due to inherent properties of the gage. It was demonstrated in chapter four that as the wavelength of the pulse approaches the length of the gage, spatial aliasing and correct magnitude resolution becomes more prevalent a problem. Other transducers, such as laser interferometery should be considered to circumvent these problems.

AUTHOR INDEX

[1] Shigley, J.E. and Mitchell, L.D., *Mechanical Engineering Design*, 4th ed., McGraw-Hill, New York, p.177 (1993)

[2] Kolsky, H., An Investigation of the Mechanical Properties of Materials at Very High Rates of Strain, *Proc. Roy. Phys. Soc.*, **B 62,** pp. 676-700 (1949)

[3] Bancroft, D., The velocity of Longitudinal Waves in Cylindrical Bars, *Physical Review*, **V.59 No.59**, pp. 588-593 (1941)

[4] Woldesenbet, E. and Vinson, J., Effect of specimen geometry in high-strain-rate testing of graphite/epoxy composites, *Collection-of-Technical-Papers AIAA/ASME/ASCE/AHS/ASC Structures, Structural Dynamics*, **v2**, pp. 927-934 (1997)

[5] Frantz, C.E. and Follansbee, P.S., Wright W. T., Experimental Techniques with the Hopkinson Pressure Bar, *High Energy Fabrication, The American Society of Mechanical Engineers*, New York, pp. 229-236 (1984)

[6] Gorham, D.A. and Wu, X.J., An empirical method for correcting dispersion in pressure bar measurements of impact stresses, *Measurement Science and Technology*, **V.7 No.9**, pp. 1227-1232 (1996)

[7] Chiddister, J.L.and Malvern, L.E., Compression-Impact Tests of Aluminum at Elevated Temperatures, *Exper. Mech.*, **V.3,** p. 81 (1963)

[8] Baker, W.E. and Yew, C.H., Strain-Rate Effects in the Propagation of Torsional Plastic Waves, *J. Appl. Mech.*, **V.33,** p. 917 (1966)

[9] Lindholm, U.S. and Yeakly, L.M., High Strain-Rat Testing: Tension and Compression, *Exper. Mech.*, **V.8**, p. 1 (1968)

[10] Staab, G.H. and Gilat, A., A Direct-tension Split Hopkinson Bar for High Strain-rat Testing, *Exper. Mech.*, **V.31**, pp. 232-235 (1991)

[11] Bertholf, L.D. and Karnes, C.H., Two-Dimnsional Analysis of the Split Hopkinson Pressure Bar System, *J. Mech. Phys. Solids*, **V.23**, pp. 1-19 (1975)

[12] Graff, K.F., *Wave Motion in Elastic Solids*, Dover, New York, pp. 80-82 (1991)

[13] Graff, K.F., *Wave Motion in Elastic Solids*, Dover, New York, pp. 95-100 (1991)

[14] Pochhammer, L., Über die Fortpflanzungsgeschwindigkeiten kleiner Schwingungen in einem unbegrenzten istropen Kreiszylinder, *J. reine angew. Math*, **81,** pp. 324-336 (1876)

[15] Love, A.E.H., *A treatise on the mathematical theory of elasticity*, Dover Publications, New York, p. 428 (1944)

[16] Davies, R.M., A critical study of the Hopkinson pressure bar, *Phil. Trans. R. Soc.*, **A240**, pp. 375-457 (1948)

[17] *CRC Handbook of Tables for Applied Engineering Science*, 2nd ed., CRC Press, p. 621 (1976)

[18] Chapra, S.C. and Canale, R.P., *Numerical Methods for Engineers*, 2nd ed., McGraw-Hill, p. 526 (1988)

[19] Dowling, D.E., *Mechanical Behavior of Materials*, Prentice Hall, New Jersey, p.174 (1993)

VITA

Michael Adam Kaiser

Michael Kaiser was born on December 13, 1971 in Maryland. His parents Michael and Sally Kaiser raised him in the lovely town of Annapolis. After graduating from Annapolis Senior High School in 1989, Michael pursued his interest in classical piano performance at the University of Maryland. Michael's curiosity in engineering outweighed his desire to become a musician, so he transferred to Virginia Tech's Mechanical Engineering department from which he received his Bachelor of Science in May of 1996. Immediately following his undergraduate work, Michael continued his education in the Masters program at Tech.

The requirements for the degree of Master of Science in Mechanical Engineering will be met in May of 1998. Mr. Kaiser is anticipating beginning his doctorate work in mechanical engineering, directly following his masters.